THE ASTROPHYSICAL JOURNAL, 399:76–93, 1992 November 1

INFRARED EMISSION AND MASS LOSS FROM EVOLVED STARS IN ELLIPTICAL GALAXIES

G. R. KNAPP AND J. E. GUNN
Princeton University Observatory, Department of Astrophysical Sciences, Peyton Hall, Princeton University, Princeton, NJ 08544
AND
C. G. WYNN-WILLIAMS
Institute for Astronomy, University of Hawaii, 2680 Woodlawn Drive, Honolulu, HI 96822
Received 1991 November 26; accepted 1992 May 4

ABSTRACT

Small aperture 10.2 μm measurements of normal elliptical galaxies show that for almost all of these galaxies the 12 μm emission seen by *IRAS* is extended on the scale of the galaxy. NGC 1052 and NGC 3998 are exceptions to this; much of their 10–12 μm emission comes from the inner regions of the galaxies and may be associated with their active nuclei, as is the case for many radio galaxies. The distribution of the infrared light and the infrared colors of elliptical galaxies suggest that the most plausible source of the 12 μm emission is photospheric and circumstellar emission from cool evolved red giant stars. The 12 μm emission is well in excess of that expected from photospheric emission alone; about 40% of it probably comes from circumstellar dust. The 12 and 2.2 μm measurements are used to derive a total mass-loss rate of $0.0021\ L_{2.2}/L_{\odot}\ M_{\odot}\ \mathrm{Gyr}^{-1}$ for the evolved giant stars in elliptical galaxies, in excellent agreement with earlier and completely independent estimates based on optical luminosities and stellar evolutionary considerations.

Subject headings: galaxies: elliptical and lenticular, cD — galaxies: stellar content — infrared: galaxies — stars: late-type — stars: mass loss

1. INTRODUCTION

This paper discusses the origin of the 10–12 μm infrared emission from bright nearby elliptical galaxies and its use as a diagnostic of nonthermal nuclear activity, the stellar populations in early-type systems and the rate of dust injection into the interstellar medium. Elliptical galaxies are generally understood to contain a single age coeval stellar population formed during the initial collapse of the protogalaxy (e.g., Tinsley & Gunn 1976); most of the bolometric (and visible) luminosity of the present-day galaxy is contributed by stars of mass $\sim 1\ M_{\odot}$ which are currently evolving from the main sequence through the red giant phase (Rose & Tinsley 1974; Gunn, Stryker, & Tinsley 1981). Recent observations and modeling have suggested some modification of this picture, however. Gunn & Dressler (1989) show that rich clusters of galaxies at moderate redshift ($z \sim 0.4$) contain a greater number of star-forming galaxies than do nearby clusters. Stellar population models of many elliptical galaxies do not reproduce the observed colors and spectra without a small contribution from main-sequence stars more massive than spectral type G (Pickles 1985; Rose 1985; O'Connell 1986), although Walsh (1990) finds that this conclusion is strongly dependent on the stellar evolution isochrones used in the modeling. Detailed surface photometry of nearby elliptical galaxies shows that some of them (e.g. NGC 3928, Tanaguchi & Watanabe 1987, and IC 1459, Goudfrooij et al. 1990) have indications of star formation in their central regions, and many nearby ellipticals also contain small amounts of cold interstellar gas (Knapp, Turner, & Cunniffe 1985; Schweizer 1987; Lees et al. 1991). However, the model of an elliptical galaxy as a system containing mostly old stars provides a reasonable first order approximation to the observations, and this paper discusses the 10–12 μm emission from elliptical galaxies in this context.

The contribution of luminous K and M stars to the stellar population in elliptical galaxies has been studied using near-infrared (1 to 2 μm) photometry (Frogel et al. 1975; Grasdalen 1975; Frogel et al. 1978; Persson, Frogel, & Aaronson 1979; Aaronson, Persson, & Frogel 1981; Glass 1984; Glass & Moorwood 1985; Impey, Wynn-Williams, & Becklin 1986). The study of the evolved stellar population is of interest not only because these stars emit most of the light but because stars lose large amounts of mass during the red giant phase in the form of cool dusty winds which inject gas and dust into the interstellar medium. While the photospheric emission from cool M giants peaks in the 1 to 3 μm range, circumstellar dust has a lower temperature and its emission peaks in the 5 to 20 μm region of the spectrum. Thus examination of the infrared emission near 10 μm from elliptical galaxies can be used to estimate the injection rate of dust (and by inference gas) into the interstellar medium (Jura 1986; Soifer et al. 1986; Gillett et al. 1988).

At present, only limited observational data for elliptical galaxies exist at 10 and 12 μm. Impey, Wynn-Williams, & Becklin (1986, 1990, hereafter Papers I and II) have observed the inner regions of a large sample of elliptical galaxies, both radio-quiet and radio-loud, at 10 μm. The *IRAS* all-sky survey (Neugebauer et al. 1984) detected weak emission at 12 μm from many nearby ellipticals (Jura 1986) and the sensitivity can be increased over that of the *IRAS* Point Source Catalog (Version 2, 1988) by factors of several by averaging the data (Jura et al. 1987; Knapp et al. 1989). There are, however, several possible origins of the 12 μm emission from elliptical galaxies in addition to emission from evolved giant stars. First, it could arise from nonequilibrium emission from small interstellar grains, as is the case for spiral galaxies (e.g. Boulanger et al. 1988). Many elliptical galaxies appear to contain small amounts of interstellar dust–the *IRAS* data show that weak emission at 100 μm, most likely due to cool interstellar dust, is present in about 50% of normal ellipticals. It could also be due to the presence of active nuclei in elliptical galaxies, either because of nonthermal

emission from the active nucleus itself or because of a small dusty region heated by the active nucleus.

The next three sections of this paper are therefore concerned with deciding among the possible origins of the 12 μm emission from elliptical galaxies. In § 2, the *IRAS* colors of ellipticals are compared with those of spiral galaxies, and it is shown that the 12 μm emission is well in excess of that expected from interstellar dust for most elliptical galaxies. In § 3, we describe small-aperture observations at 10 μm made with the Infrared Telescope Facility (IRTF) on Mauna Kea, Hawaii; these are discussed in § 4, and show that in almost all cases the 12 μm emission from elliptical galaxies in extended on the scale of the optical galaxy and is therefore not due to active nuclei. Comparison with the surface brightness model of de Vaucouleurs (1948) shows that the 12 μm emission is distributed like the starlight and thus most likely arises from evolved stars and their dusty circumstellar envelopes. In § 5, we compared the 12 and 2.2 μm flux densities of the elliptical galaxies with those of Galactic evolved stars to examine the evolved stellar population of elliptical galaxies and to estimate the dust and gas injection rates. The conclusions are given in § 6. Appendix A discusses the derivation of total flux densities and the de Vaucouleurs-law (1948) effective radii from available 2.2 μm multiaperture photometric data, and Appendix B discusses the extrapolation of the *IRAS* photometry to total asymptotic flux densities using the de Vaucouleurs-law surface brightness model.

2. INTERSTELLAR DUST IN ELLIPTICAL GALAXIES

In this section we examine the possibility that the 12 μm emission is due to dust by comparing the *IRAS* colors of elliptical galaxies with those of spirals. *IRAS* observed the sky at wavelengths of 12, 25, 60, and 100 μm; normal spiral galaxies are most strongly detected at 100 μm, and the infrared emission at this wavelength is generally considered to be due to cool interstellar dust heated by the ambient ultraviolet interstellar radiation field (de Jong et al. 1984; Helou 1986) to an equilibrium temperature of about 20 K (Draine & Lee 1984). However, the emission at shorter wavelengths (12 and 25 μm) is much stronger than expected from this model, and is attributed to emission from small grains heated intermittently to nonequilibrium temperatures by individual interstellar ultraviolet photons (Sellgren 1984; Wynn-Williams & Becklin 1985; Draine & Anderson 1985: Boulanger et al. 1988). This process also contributes significantly to the 60 μm flux density. In this section we ask whether it is likely that the 12 μm emission observed from elliptical galaxies can be attributed to the presence of small grains.

The presence of small amounts of dust in many elliptical galaxies is suggested by weak 100 μm emission (Jura et al. 1987; Marston 1988; Knapp et al. 1989; Knapp, Bies & van Gorkom 1990; Paper II; Knapp & Patten 1991). It is thus plausible to attribute the 12 μm emission also to interstellar dust, i.e., to small grains. If this were so, the conclusion would be of considerable interest, for comparison between the 12 μm and longer wavelength emission could be used to investigate the grain size distribution and the interstellar radiation field in elliptical galaxies. The question discussed in this section is whether the 12 to 100 μm flux density ratio in elliptical galaxies is similar to that in spiral galaxies, where emission at both wavelengths is dominated by the presence of interstellar dust. Figure 1*a* shows a plot of S_{12} versus S_{100} for the spiral galaxies in the Virgo Cluster from the survey by Helou et al. (1988); this sample is used because all of the galaxies are at the same distance. As Figure 1*a* shows, there is a very tight correlation between these two flux densities, reflecting perhaps a similarity in the grain size spectrum and distribution between the diffuse the dense interstellar medium for spiral galaxies. The galaxies in the sample range in morphological type from Sa through Sdm. The mean relationship between the 12 and 100 μm flux densities in Figure 1*a* is

$$S_{12\,\mu m} = 0.042 S_{100\,\mu m} \quad (1)$$

Figure 1*b* shows S_{12} versus S_{100} for most of the elliptical galaxies from Knapp et al. (1989) for which 12 μm emission is detected at greater than the 2 σ level. For the galaxies with larger angular sizes the total flux densities, integrated over the area of the galaxy, are plotted. The few infrared brightest ellipticals (NGC 1275 at 900, 2650; NGC 5128 at 2.3×10^4, 4.9×10^5; NGC 6524 at 270, 7900) in the sample lie outside the plotted range and are excluded for clarity of plotting. The value plotted for the 100 μm flux density is either the observed value (for galaxies detected above the 2 σ level) or is the 2 σ upper limit. Also plotted in Figure 1*b* is the mean relationship for spiral galaxies from Figure 1*a*.

Almost all of the elliptical galaxies plotted in Figure 1*b* are very faint at 100 μm and have a 12 to 100 μm flux density ratio which is well in excess of that seen for spiral galaxies. In spirals, almost all of the radiation at 12 and at 25 μm is due to nonequilibrium heating of small grains by starlight, and this process contributes significantly to the emission at 60 μm also, resulting, among other things, in a 60 to 100 μm color which does not give a reliable dust temperature (Draine & Anderson 1985; Draine 1990). Kim (1989) has discussed the possibility that dust in elliptical galaxies undergoes nonequilibrium heating by X-ray photons (cf. Canizares, Fabbiano, & Trinchieri 1987). One might expect the intermittent heating by X-rays and the resulting nonequilibrium emission in ellipticals to be more pronounced and to involve larger grains than in spirals, and this might account for the observed 12 μm excess.

Were this the case, the color temperature, measured by the 60/100 μm flux ratio, would likely be larger in elliptical galaxies than in spiral galaxies. Figures 2*a* and 2*b* show, respectively, the 60 and 100 μm flux density plots for spiral galaxies, again using the Virgo cluster sample of Helou et al. (1988), and for elliptical galaxies (detected at greater than 3 σ at both 60 and 100 μm) from the survey by Knapp et al. (1989). The best-fit linear relation for the spiral galaxies is $S_{60\,\mu m} = 0.46 \pm 0.01\, S_{100\,\mu m}$. For the ellipticals, if we omit the peculiar dusty radio galaxies NGC 1275 and NGC 5128 (which in any case have such large fluxes that they completely dominate the regression), the corresponding coefficient is 0.44 ± 0.02, insignificantly different from the spirals. It is clear from a comparison of Figures 2*b* and 1*b*, however, that the regression is dominated by ellipticals with "normal" (i.e., spiral-like) 12 to 100 μm flux ratios, because those are the galaxies with the largest 100 μm fluxes in the sample. If one restricts the sample to those objects which typically show large 12 to 100 μm ratios, say to those with fluxes less than 2000 mJy at 100 μm, the 60 to 100 μm ratios are smaller. For this sample the coefficient is 0.33 ± 0.02. If one goes further and deletes the galaxies for which the 12 μm emission is likely to be dominated by the emission from cool dust (thus eliminating those galaxies with the lowest 12 to 100 μm ratios) the 60 to 100 μm ratio is lower yet, the coefficient dropping to 0.27 ± 0.03. In fact, the few elliptical galaxies which are bright 100 μm sources have values of S_{12}/S_{100} which are systematically less than the mean

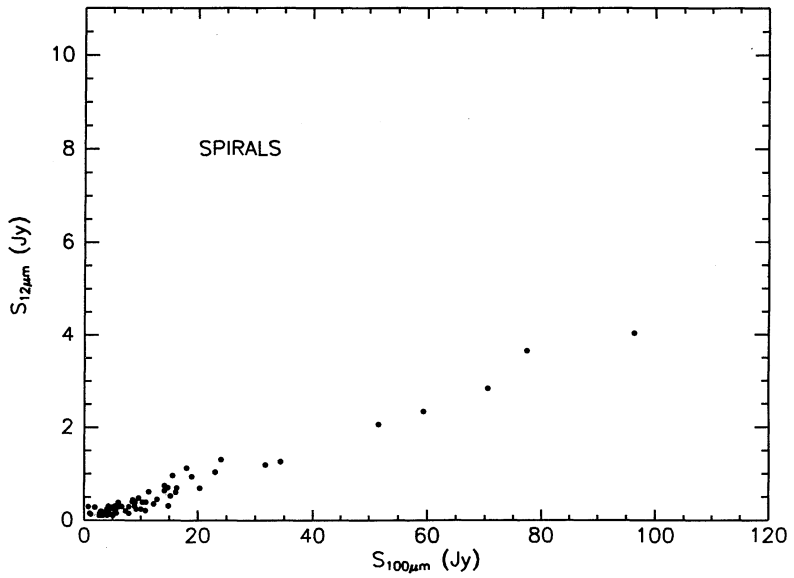

FIG. 1*a*

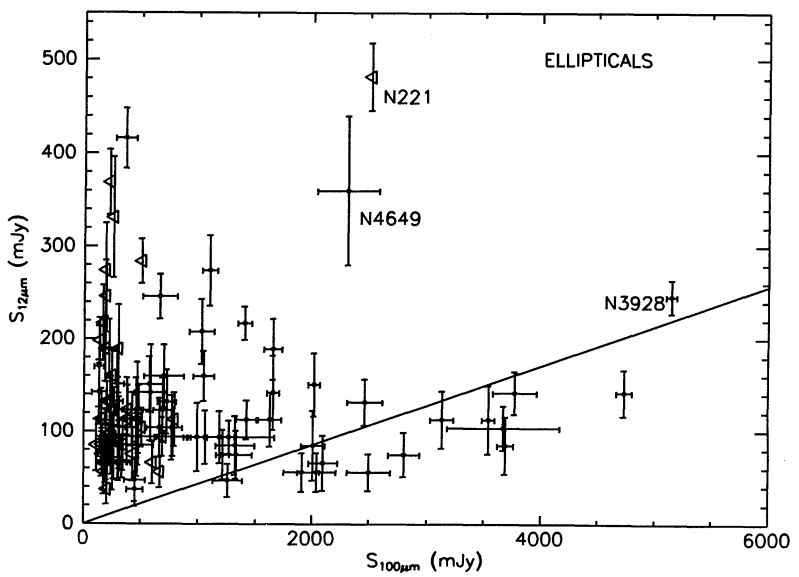

FIG. 1*b*

FIG. 1.—(*a*) Integrated 12 μm flux density vs. integrated 100 μm flux density for spiral galaxies in the Virgo Cluster from Helou et al. (1989). (*b*) 12 μm flux density vs. 100 μm flux density for elliptical galaxies detected at 12 μm (at greater than the 2 σ level) from Knapp et al. (1989). The error bars shown in each coordinate are 1 σ. The upper limits for galaxies detected at 100 μm are 2 σ. The mean relationship for spirals from Fig. 1*a* is shown by the line. The data for NGC 3928 are discussed in the text (§ 3).

relationship for spiral galaxies, as one might expect from the lower S_{60}/S_{100} ratios. Thus, if anything, the elliptical galaxies are "cooler" than are the spiral galaxies, and it seems very unlikely that nonequilibrium emission from hot interstellar dust grains is responsible for the excess 12 μm emission.

The second possibility, which is considered in the next two sections, is that the excess 12 μm emission is due to the presence of small nuclear sources in elliptical galaxies. The obvious test of this hypothesis is to determine the extent of the 12 μm emission. The *IRAS* observations alone cannot answer this, for the beam is fairly large (45″ in the scan direction). In Paper I small-aperture flux densities for many early-type galaxies were measured at the adjacent wavelength of 10 μm. We undertook to supplement these observations with further small aperture 10 μm observations of elliptical galaxies which are relatively strongly detected at 12 μm (Knapp et al. 1989). These observations are described in the next section (§ 3); in § 4 the results are discussed and, together with those of Paper I were used to examine whether the 12 μm emission is pointlike or extended.

3. OBSERVATIONS AT 10 μm

3.1. *Observational Results*

The observations were carried out on the nights of 1990 March 17, 18, and 19 using the 3 m telescope of NASA's Infrared Telescope Facility (IRTF) on Mauna Kea, Hawaii. The

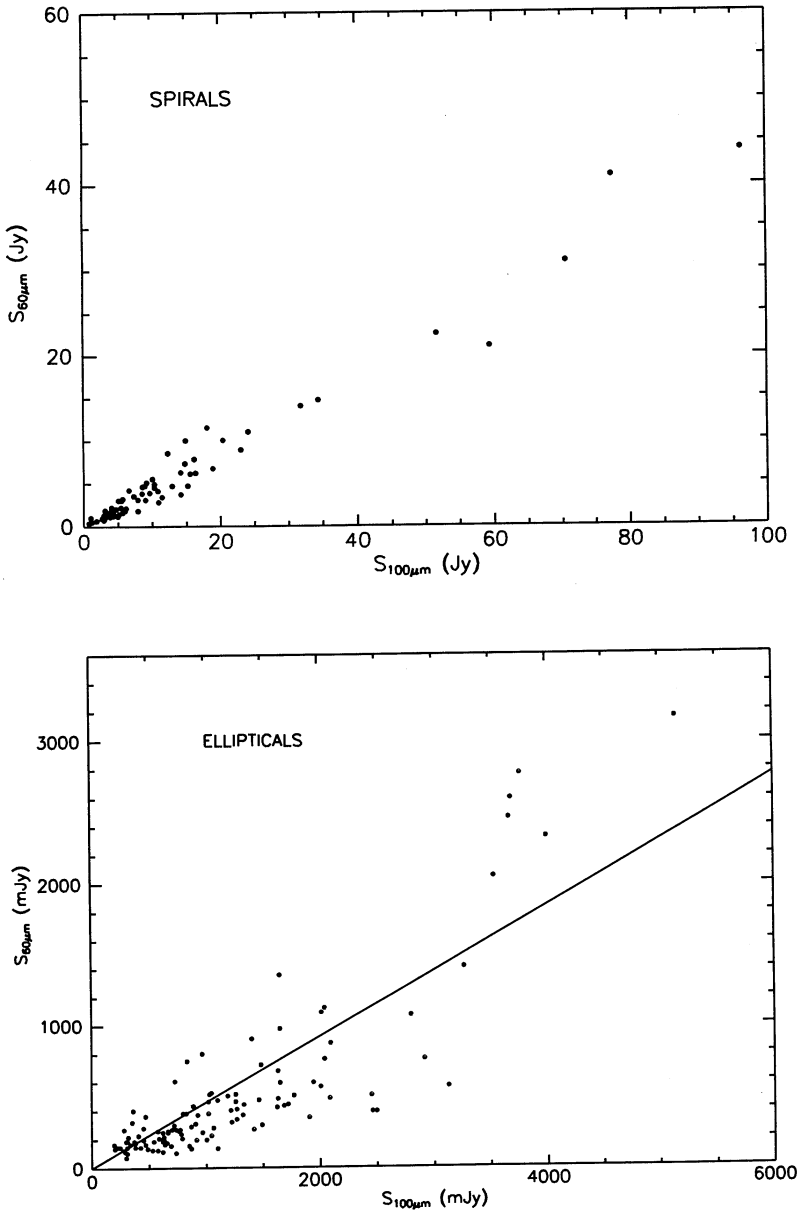

FIG. 2.—(*a*) 60 μm flux density vs. 100 μm flux density for spiral galaxies in the Virgo cluster, from the sample of Helou et al. (1988). (*b*) 60 μm flux density vs. 100 μm for elliptical galaxies from the sample of Knapp et al. (1989). The galaxies included are those for which both the 60 μm and the 100 μm flux densities are detected at greater than the 3 σ level. The mean relationship for spirals from Fig. 2*a* is shown by the line.

weather was clear throughout the observing run. The observations were made with a liquid-helium cooled bolometer mounted at the Cassegrain focus with a wide band 8–13 μm filter centered at 10.2 μm and with a circular aperture of 5″.7 on the sky. The data were taken by chopping at a rate of 13 Hz with a beam throw of 30″ north-south. The object to be observed was placed alternately in the two aperatures and the signals averaged. The typical integration time used was 30 minutes per galaxy. The galaxies were acquired by centering on the optical nucleus using a Quantex TV camera. They were selected to be optically bright galaxies with 12 μm flux densities greater than 80 mJy (Knapp et al. 1989) and mostly of morphological type E. Together with the observations of Paper I these form an almost complete set for elliptical galaxies which are bright at 12 μm.

The flux densities were measured by comparison with observations of standard cool stars observed at similar air masses to the galaxies. These observations of standard stars were also used to align the optical and infrared beams before each galaxy was observed. The flux densities of the standard stars are measured on a scale where the magnitude of α Lyrae is 0.0 mag at all wavelengths and its flux density at 10.2 μm is 37 Jy. The resulting flux densities for the galaxies were not corrected for possible differences in spectral shape between the galaxies and the standard stars. Twenty-eight positions were measured in 27 galaxies. The results are given in Table 1, which lists for each

TABLE 1

10 μm OBSERVATIONS OF EARLY-TYPE GALAXIES

Galaxy	α(1950)	δ(1950)	Type	B_T	S(10.2)	σ(10.2)	S(12)
NGC 1700	04h54m28s1	−04°56′30″	E4	12.5	13.4	7.6	123
NGC 2292	06 45 39.0	−26 41 24	E/S0	11.2	2.1	7.9	133
NGC 2320	07 01 49.5	+50 39 24	E	12.8	13.7	7.4	114
NGC 2380	07 21 54.0	−27 25 47	E	12.1	8.7	8.3	95
NGC 2663	08 43 08.0	−33 36 42	E3	11.5	2.9	10.7	85
NGC 2685	08 51 41.2	+58 55 30	S0p	11.9	−22.9	13.9	104
NGC 2768	09 07 45.2	+60 14 40	E6	11.1	5.8	8.4	76
NGC 2831[a]	09 16 43.3	+33 57 20	E0	14.6	−6.6	7.3	76
NGC 2832[a]	09 16 43.7	+33 57 45	E3	12.5	−15.7	10.5	
NGC 3070	09 55 27.0	+10 36 01	E	13.3	0.5	10.0	114
NGC 3250	10 24 21.0	−39 41 18	E3	12.0	−18.2	19.0	331
NGC 3265	10 28 19.1	+29 03 13	E4	13.9	41.1	6.8	85
NGC 3557	11 07 35.0	−37 16 00	E3	11.5	5.8	10.1	246
NGC 3585	11 10 50.0	−26 28 48	E7	10.8	8.6	11.5	114
NGC 3706	11 27 17.0	−36 07 00	E4/S0	12.2	10.1	12.0	76
NGC 3812	11 38 31.3	+25 05 54	E	13.7	−6.3	8.9	369
NGC 3923	11 48 29.7	−28 31 40	E4/S0	10.8	0.4	10.0	123
NGC 3928[a]	11 49 10.6	+48 57 38	E0	12.9	41.5	6.0	246
NGC 3998	11 55 21.4	+55 43 57	S0	11.5	58.1	8.8	133
NGC 4015	11 56 08.6	+25 18 53	E + E	13.7	−3.0	8.7	104
NGC 4278	12 17 36.5	+29 33 26	E1	11.1	13.6	4.6	142
NGC 4339	12 21 01.3	+06 21 32	E0	12.4	−2.9	10.8	133
NGC 4458	12 26 25.9	+13 31 10	E	12.9	9.5	8.0	95
NGC 5363[a]	13 53 36.3	+05 29 58	I0	11.1	41.7	10.6	189
NGC 5363[b]	13 53 36.1	+05 29 55			11.5	10.7	
NGC 5666	14 30 43.3	+10 43 47	Ec	13.0	−4.1	12.6	114
NGC 5838	15 02 54.6	+02 17 37	S0	11.8	19.1	6.8	123
NGC 5866	15 05 07.8	+55 57 16	S0	10.9	34.1	5.7	303

[a] See notes in § 3.2.
[b] Foreground star.

galaxy the position, the morphological type, the blue asymptotic magnitude, the 10.2 μm flux density and the rms noise at 10.2 μm, in mJy, and the 12 μm flux density measured by *IRAS* from Knapp et al. (1989). (The values in that paper are rounded.) As can be seen from Table 1, seven of the galaxies were detected at about the 3 σ level or greater at 10.2 μm.

Test observations of blank sky discussed in Paper I showed that the beam responses are well balanced and that there are no positive or negative biases in the data. Since we used the same instrumental set up and observed model in our work, we are confident that the detections made in this paper are real. In Figure 3 we plot the histogram of observed flux densities from Table 1. The Gaussian curve shown in Figure 3 has the mean dispersion of our observations (Table 1, col. [7]). There is an excess of eight positive signals over the value predicted from this Gaussian. This compares well with the seven 3 σ detections in Table 1, and shows that the rms noise values quoted in Table 1 are a reasonable measure of the flux uncertainties.

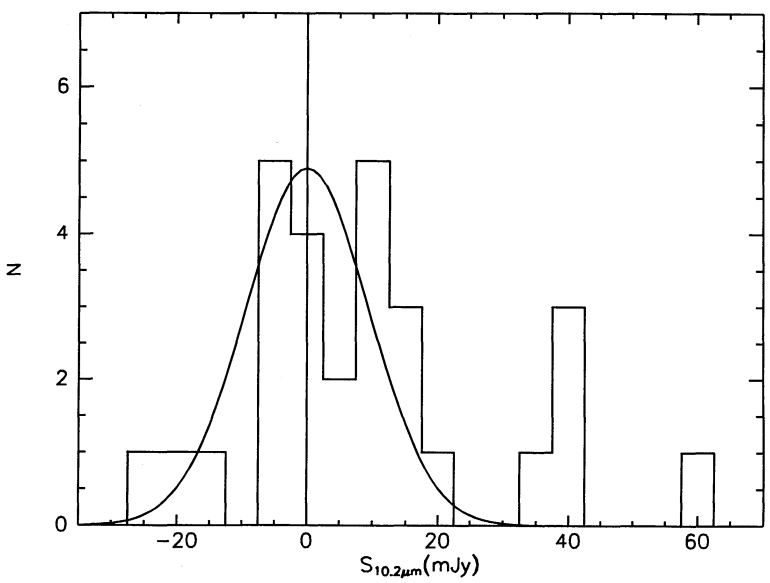

FIG. 3.—Histogram of observed 10.2 μm small-aperture flux densities measured at IRTF. The Gaussian is fit to the points with $S_{10\,\mu m} < 0$

3.2. *Individual Galaxies*

NGC 2831/NGC 2832.—The nuclei of both galaxies of this elliptical pair were observed. The nuclei are separated by about 45″ (the positions in Table 1 are taken from Grasdalen 1975) and are not resolved by the 45″ beam of the *IRAS* observations. We detected 10 μm emission from neither galaxy.

NGC 3928.—The IRTF observations detected 10 μm emission from the inner regions of this galaxy showing that about $\frac{1}{6}$ of the 12 μm flux density is emitted by the central few arcseconds of the galaxy. NGC 3928 is classified as E0 but proves to be quite unusual upon closer examination; it is very blue for an elliptical galaxy ($B - V = 0.66$ mag, Huchra 1977) and embedded in the bulge is a small tightly wound spiral disk (van den Bergh 1980; Tanaguchi & Watanabe 1987). The galaxy also contains cold interstellar gas in the form of molecules (CO emission has been detected by Gordon 1990), H I (Thuan & Martin 1981), and dust—the *IRAS* 100 μm flux density is relatively large and the 12 to 100 μm ratio is similar to that found in spiral galaxies (Fig. 2). Further, NGC 3928 appears to be forming stars in its nucleus and disk; Tanaguchi & Watanabe (1987) show that the nuclear emission line spectrum resembles that of an H II region. The galaxy is also a weak radio source (Wrobel & Heeschen 1991) and the radio to infrared luminosity ratio is similar to that found in the disks of spiral galaxies (Walsh et al. 1989) indicating the presence of star formation. The galaxy has a bright star-forming core of diameter about 4″ (van den Bergh 1980; Tanaguchi & Watanabe 1987); the 10 μm emission (Table 1) may arise from hot dust in this region.

NGC 4278.—Observations of this galaxy are also given in Paper I. Our flux density of 13.6 $\pm$ 4.6 mJy agrees well with the previous measurement of 18.5 $\pm$ 8.4 mJy.

NGC 5363.—This galaxy is variously classified as IO or E (peculiar), and appears to be an elliptical galaxy with a minor axis dust lane (Bertola 1987). Emission at 10 μm was detected from the nucleus (Table 1). During the observations a second brighter optical source was seen on the Quantex camera about 4″ southwest of the nucleus. In case it should prove to be of interest, this object was also observed at 10 μm but was not detected—the position given in Table 1 was measured by offsetting from the positions of the stars SAO 120182 and SAO 120196. The position of the nucleus itself was also measured relative to that of the SAO stars and found to be within 1″ of that given by Dressel & Condon (1976). This new position is given in Table 1. Sharples et al. (1983) give optical images of NGC 5363 and identify the brighter source as a foreground galactic star.

The relevant data for the rest of the paper are assembled in Table 2, which contains data for all the galaxies which have one of the following properties:

1. A 3 σ detection by *IRAS* at 12 μm, or
2. A measurement at 10.2 μm from this Paper or Paper I, or
3. Enough multiaperture 2.2 μm data to determine a de Vaucouleurs effective radius (see Appendix A and the discussion in the next two sections).

The galaxy name is given in column (1), the type from Knapp et al. (1989) in column (2), the *IRAS* 12 μm flux or its 2 σ upper limit in column (3), and that flux corrected for cool dust according to equation (1) in column (4). If the corrected flux is less than half the total, a double asterisk (**) is entered, and if the correction is based on a 100 μm upper limit, in which case the 100 μm flux is taken to be the 1 σ limit, the entry is preceeded by an asterisk (*). A glance through the table indicates that these uncertain corrections are nearly always very small, in most cases less than 10%; the large corrections are invariably based on 100 μm detections. Column (5) gives the 12 μm standard deviation, and columns (6) and (7) the 10.2 μm flux and its standard error. Column (8) gives the reference for the 10.2 measurement; P1 is Paper I, and T1 is Table 1, this paper. The effective radii and total 2.2 μm flux density (cf. Appendix A) derived from 2.2 μm photometry are listed in columns (9) and (10). We defer discussion of the rest of the table and some special cases contained in it until we are ready to make use of the data.

These data will be used in the next section to examine the distribution of the 12 μm emission in elliptical galaxies, and in § 5 to show that the emission arises largely from the photospheres and circumstellar envelopes of late-type giant stars.

4. THE EXTENT OF THE 12 μm INFRARED EMISSION FROM ELLIPTICAL GALAXIES

We will in this section compare the small-aperture 10.2 μm observations described in the last section and those from Paper I with the 12 μm *IRAS* flux densities from the same galaxies, and show that in most cases the 10–12 μm emission is extended on the scale of the galaxy and indeed that the data are consistent with that emission being distributed like the starlight for most galaxies.

Figure 4 shows the small-aperture 10 μm flux density or its 2 σ upper limit versus the 12 μm flux density observed by *IRAS* for two samples of galaxies. These are, first, the nearby bright elliptical galaxies from the present measurements (Table 1) and from Paper I for galaxies for which the 12 μm emission was detected by *IRAS* (this is the case for all of the galaxies in Table 1 and for the majority of those from Paper I). These galaxies are plotted as filled and open circles (for detections) and filled and open triangles (for 2 σ upper limits at 10.2 μm). The second sample contains data from the radio galaxies from Paper II for which *IRAS* detected 12 μm emission, and are plotted as crosses. We will discuss the distinction between the open and filled symbols later.

Also shown in Figure 4 is the line corresponding to equal small- and large-aperture flux densities color-corrected for the difference in observational wavelengths by assuming $S_{10.2} = 0.7S_{12}$ (Hill, Becklin, & Wynn-Williams 1988). Figure 4 shows that two of the nearby bright elliptical galaxies (NGC 1052 and NGC 3998, both of which have strong nuclear radio sources and nuclear optical emission) and several of the radio galaxies emit most of their 10–12 μm flux from their nuclear regions. For all of the remaining elliptical galaxies the small- aperture flux density, while roughly proportional to the large aperture flux density, is only a small fraction of the total flux density of the galaxy, and therefore most of this flux originates in an extended region.

An interesting question this observation raises is whether the extended 10–12 μm emission is in fact distributed like the starlight, as it would be if it arises either from the photospheres of cool stars or from circumstellar dust. In the latter case, there might be differences arising from the effects of metallicity gradients on the stellar temperatures and/or the dust ejection rates, but our data are almost certainly not good enough to investigate these effects. We will use the small (IRTF) and large (*IRAS*) aperture observations to examine this question and do this by comparing the observed ratio of these fluxes to that

TABLE 2

FLUX DENSITIES AND DERIVED QUANTITIES FOR THE ELLIPTICAL SAMPLE

Galaxy	type	S_{12}	$S_{12,c}$	σ_{12}	$S_{10.2}$	$\sigma_{10.2}$	ref	r_e	$S_{2.2}$	f_{IRAS}	f_{IRTF}	R	σ_R	Notes
N0205	E5p	113	**	31	−3.4	6.1	P1							
N0221	E2	482	*429	36	63.6	5.7	P1	26.4	4920	0.65	0.078	0.123	0.014	1,2
N0584	E4/S0	< 88			14.0	6.4	P1	31.3	880	0.61	0.065			2
N0596	E1	< 66			16.5	7.3	P1	28.1	480	0.64	0.073			2
N0636	E3	123	*117	24	5.8	6.4	P1	18.9		0.72	0.112	< 0.107		1,3
N0720	E5	85	*82	28	4.6	5.5	P1	39.5		0.55	0.049	< 0.102		1,3
N1052	E3	217	158	18	117.6	11.3	P1	16.1	560	0.76	0.130	0.588	0.075	5
N1344	E5	< 54						65.2	1350	0.43				2
N1379	E0	< 48						47.4	580	0.51				2
N1395	E2	132	119	26	20.2	7.3	P1	101.3	2750	0.33	0.015	0.072	0.030	1,2
N1399	E1	94	82	23				124.7	5360	0.29				2
N1400	E/S0	< 72						25.4	620	0.66				2
N1404	E2	94	83	41				83.6	3280	0.37				2
N1407	E0	113	95	29	4.3	7.2	P1	125.0	3460	0.29	0.011	< 0.053		1,2
N1453	E2	104	76	32				19.7	380	0.72				2
N1549	E1	94	87	18				13.0	760	0.80				2
N1587	E + E1	113	*104	45	13.4	5.8	P1	18.2	270	0.74	0.116	0.125	0.074	1,2
N1600	E4	< 28						59.6	770	0.46				2
N1700	E4	123	*114	27	13.4	7.6	T1	14.9	370	0.78	0.140	< 0.138		1,2
N2292	E/S0	132	**	25	2.1	7.9	T1							
N2300	E3	85	*81	18				27.0	660	0.65				2
N2320	E	113	**	21	13.7	7.4	T1	43.0		0.53	0.045	< 0.099		3
N2380	E	94	*79	21	8.7	8.3	T1	43.0		0.53	0.045	< 0.134		1,3
N2434	E0	< 38						23.7	510	0.68	0.046			2
N2634	E1	< 38						14.3	150	0.78				2
N2663	E3	85	*80	23	2.9	10.7	T1	40.9	1280	0.55	0.048	< 0.198		1,2
N2672	E1 + E0	< 70						46.0	520	0.52				2
N2685	S0p	104	**	31	−22.9	13.9	T1							
N2693	E2	< 58			18.4	7.0	P1							
N2768	E6	75	**	27	2.5	8.7	P1	45.4	1100	0.52	0.042	< 0.172		
N2831/2	E0 + E3	75	**	26										6
					−6.6	7.3	T1							
					−15.7	10.5	T1							
N2974	E4	< 42						13.9	430	0.79				2
N2986	E2	< 52						25.4	580	0.66				2
N3070	E	113	*102	37	0.5	10.0	T1	15.0		0.77	0.139	< 0.195		1,3
N3136	E4	85	*78	26				26.7	740	0.65				2
N3158	E3	< 62			3.4	8.7	P1	6.1	90	0.91	0.303			2
N3193	E2	< 66						16.5	390	0.76				2
N3250	E3	331	*325	65	−18.2	19.0	T1	28.3	660	0.64	0.072	< 0.105		1,2
N3265	E4	85	**		41.1	6.8	T1							
N3268	E2	< 64						33.7	550	0.60				2
N3309	E2	< 50						39.3	430	0.56				2
N3377	E6	104	90	33	0.0	7.8	P1	20.1	250	0.72	0.105	< 0.154		1,2,4
N3379	E0	246	*241	39	15.0	7.2	P1	31.2	1890	0.61	0.065	0.053	0.027	1,2
N3557	E3	250	*239	24	5.8	10.1	T1	23.9	800	0.68	0.087	< 0.078		1,2
N3585	E7	113	*109	33	8.6	11.5	T1	34.9	1460	0.59	0.057	< 0.172		1,2
N3610	E5	< 68			16.1	7.8	P1							
N3613	E6	< 50			13.7	8.4	P1	17.2	410	0.75	0.123			2
N3640	E2	< 124			2.8	6.3	P1	34.4	820	0.59	0.058			2
N3706	E4/S0	75	66	31	10.1	12.0	T1							
N3812	E	369	*364	35	−6.3	8.9	T1							
N3842	E3	85	**	32				27.9	230	0.64				
N3904	E2	94	73	31				30.0	690	0.62				2
N3923	E4/S0	123	*117	36	0.4	10.0	T1	78.0	2530	0.39	0.021	< 0.091		1,2
N3928	E0	246	**	18	41.5	6.0	T1							7
N3962	E1	< 68						31.6	690	0.61				2
N3998	S0	132	89	23	58.1	8.8	T1	7.3	460	0.89	0.264	0.560	0.129	5
N4015	E + E	104	71	35	−3.0	8.7	T1	21.2		0.70	0.099	< 0.167		1,3
N4261	E3	170	164	44	29.9	7.7	P1	47.7	1220	0.51	0.040	0.128	0.047	1,2
N4278	E1	142	72	40	13.6	4.6	T1	24.8	970	0.67	0.084	0.092	0.040	1,2
N4283	E0	< 100						8.3	160	0.87				2
N4339	E0	132	123	30	−2.9	10.8	T1	30.7		0.61	0.066	< 0.143		1,3
N4365	E3	151	126	30	0.0	7.5	P1	44.8	1460	0.53	0.043	< 0.075		1,2
N4374	E1	208	164	35	20.9	7.2	P1	43.7	2180	0.53	0.044	0.076	0.029	1,2

TABLE 2—*Continued*

Galaxy	type	S_{12}	$S_{12,c}$	σ_{12}	$S_{10.2}$	$\sigma_{10.2}$	ref	r_e	$S_{2.2}$	f_{IRAS}	f_{IRTF}	R	σ_R	Notes
N4387	E5	< 66						13.8	160	0.79				2
N4406	E3	151	138	35	7.0	6.4	P1	84.8	3130	0.37	0.019	< 0.045		1,2
N4458	E	94	*88	25	9.5	8.0	T1	109.9	470	0.31	0.014	< 0.075		1,2
N4468	E/S0	< 68						26.3	80	0.66				2
N4472	E2	189	*185	35	7.5	6.1	P1	115.8	6920	0.30	0.013	< 0.028		1,2
N4473	E5	274	*270	51	19.7	5.8	P1	21.7	880	0.70	0.096	0.072	0.025	1,2
N4476	E/S0	< 94			9.3	8.9	P1	65.7	280	0.43	0.027			2
N4478	E2	< 74			9.3	8.5	P1	27.9	470	0.64	0.074			2
N4486	E0	416	400	32	34.6	6.2	P1	224.5	10770	0.18	0.005	0.021	0.004	1,2
N4486b	E0	< 98						4.4	80	0.94				2
N4494	E1	< 56			9.7	10.4	P1	24.4	820	0.67	0.085			2
N4550	S0	< 58			25.1	12.3	P1							
N4552	E0	123	103	52	21.1	7.6	P1	22.1	1140	0.70	0.094	0.172	0.095	1,2
N4564	E6	< 70			20.0	8.6	P1							
N4621	E5	217	*213	41	8.0	6.1	P1	27.4	860	0.64	0.075	< 0.051		1,2,4
N4636	E0	189	*182	48	−6.2	5.8	P1	74.8	1940	0.40	0.023	< 0.035		1,2
N4649	E2	227	186	38	−11.2	9.3	P1	189.8	11960	0.21	0.006	< 0.025		1,2
N4660	E5	< 58			17.9	8.9	P1							
N4696	S0	< 52						197.8	2920	0.20				2
N4697	E6	274	227	38	25.2	5.7	P1	34.5	1510	0.59	0.058	0.078	0.021	1,2
N4742	E4	< 82						9.0	280	0.86				2
N4760	E0	< 40						16.3	210	0.76				2
N4782	E0	< 74						216.8	4350	0.19				2
N4783	E0	< 78						35.2	370	0.58				2
N4880	S0	< 34			24.0	11.5	P1							
N4889	E4	< 70						25.9	310	0.66				2
N5018	E3	189	119	33	5.8	8.7	P1	14.6	520	0.78	0.143	< 0.103		1,2
N5061	E0	132	*127	21				23.0	810	0.69				2
N5090	S0?	< 58						39.9	590	0.55				2
N5128	E	4640	**	34				88.6	12570	0.36				
I4296	E0	< 54						29.1	670	0.63				2
N5357	E2	< 46						15.9	190	0.76				2
N5363	I0	189	**	36	41.7	10.6								7
N5557	E2	< 70			22.9	9.4	P1							
N5576	E	66	58	34			P1							
N5666	Ec	113	**	37	−4.1	12.6	T1							
N5813	E1	< 56			−2.4	10.5	P1	29.7	610	0.63	0.069			2
N5838	S0	123	**	28	19.1	6.8	T1							
N5846	E0	< 44			0.5	10.5	P1	109.5	2410	0.32	0.014			2
N5866	S0	303	**	16	34.1	5.7	T1							
N5982	E3	< 40			8.9	10.5	P1	22.6	450	0.69	0.092			2
N6166	E2p	< 44						13.1	50	0.80				2
N6482	E3	66	*53	23	8.8	8.5	P1							
N6702	E3	< 62			0.2	9.1	P1	25.8	210	0.66	0.080			2
N6721	E1	< 48						18.4	210	0.73				2
N6868	E2	< 60						30.1	790	0.62				2
N6958	E1	151	**	34				6.9	240	0.90				
N7029	E6	< 50						22.5	310	0.69				2
N7052	E4	47	**	18				16.4	200	0.76				
N7196	E3	56	**	21				11.6	310	0.82				
N7562	E2	< 58						21.6	370	0.70				2
N7619	E2	< 62						24.2	500	0.67				2
N7626	E	< 92						21.0	380	0.71				2
N7796	E2	< 34						37.1	510	0.57				2

NOTES.—(1) sample 1, (2) sample 2, (3) r_e from optical data of Faber et al. 1989, (4) r_e is geometric mean of optical and 2.2 μm values, (5) active nucleus, (6) composite objects at *IRAS* resolution, (7) peculiar; see § 3.2. All flux densities are in mJy. The 12 μm densities and their 1 σ errors measured by *IRAS* are listed in cols. (3), (4), and (5); the 12 μm flux densities in col. (5) are corrected for emission from cold dust (see text). Those galaxies for which the corrections are derived from 100 μm upper limits are marked with an asterisk (*), and double asterisks (**) denote galaxies for which the correction is half or more of the uncorrected flux. The 10.2 μm flux densities and their 1 σ errors measured through an aperture of 5".7 at IRTF are given in cols. (6) and (7) . The source of the 10.2 μm data is given in col. (8) (P1: Paper I; T1: Table 1). Col. (9) gives the de Vaucouleurs effective radius in arcseconds; Col. (10) gives the 2.2 μm flux density. Col. (11) gives the fraction of the total flux density measured by the *IRAS* aperture, and col. (12) the fraction of the total flux density measured in the 5".7 IRTF aperture, assuming a de Vaucouleurs profile with the r_e in col. (9). Col. (13) gives the observed ratio R of 12 μm flux density within a 5".7 aperture to the total flux density, corrected for color (see text) and col. (14) the error in the quantity.

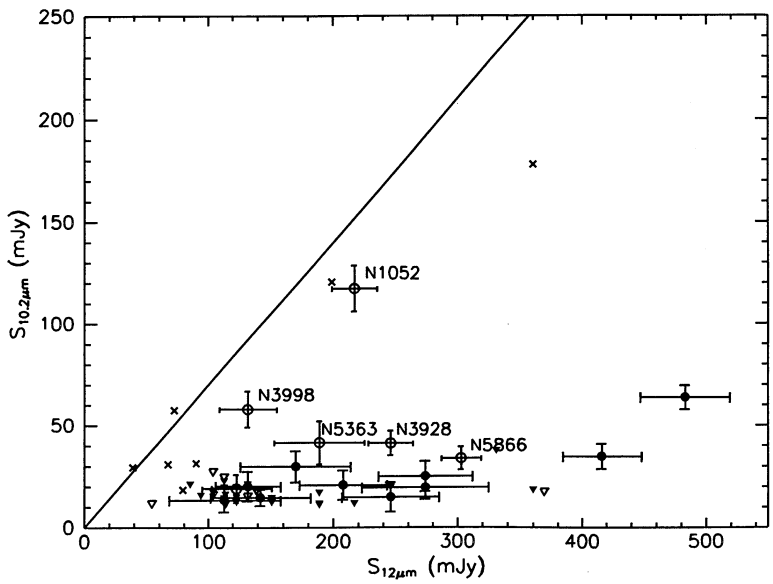

FIG. 4.—Small aperture 10 μm flux densities measured at IRTF vs. global 12 μm flux densities, from the data of Impey et al. (1986, 1990) and from the present paper. The error bars are 1 σ. 2 σ upper limits for the 10 μm flux densities are shown by inverted triangles. The crosses are radio galaxy data from Impey et al. (1990). The line represents $S_{10\,\mu m} = 0.7 S_{12\,\mu m}$, i.e., color-corrected equal flux densities.

expected if the surface brightness $I(r)$ follows the de Vaucouleurs (1948) distribution:

$$I(r) = I_e \exp\left\{-7.67\left[\left(\frac{r}{r_e}\right)^{0.25} - 1\right]\right\} \quad (2)$$

where r_e is the effective radius (containing half of the total flux) and I_e is the surface brightness at r_e.

Given a sample of galaxies with measured flux densities at some frequency in large and small apertures and values of r_e, it is clearly possible by simply integrating the de Vaucouleurs profile to ascertain whether the large and small aperture measurements are consistent with the de Vaucouleurs profile for that r_e. We will discuss how we deal with the rectangular *IRAS* beam shape and the statistics of our rather poor signal-to-noise measurements later; let us consider first a suitable sample with which to address this question.

We must clearly look at galaxies for which we have both small and large aperture data, so we begin with the set of data from this paper and Paper I (the Paper II galaxies are badly contaminated by nuclear emission and we do not consider them) for which there are *IRAS* 12 μm detections, and we exclude the two strong-nucleus galaxies NGC 1052 and NGC 3998. In order to make the comparison with the starlight, there must exist data from which the effective radius can be determined; there are only a few galaxies for which such data do not exist. We demand furthermore that the contribution from cool dust at 12 μm not dominate the emission. Thus we calculate the expected or maximum contribution to the 12 μm flux density using equation (1) with the observed or 2 σ upper limit 100 μm *IRAS* flux density, and if that is smaller than half the total 12 μm flux density, the galaxy is included. This sample contains 34 galaxies and is identified in Table 2 as "sample 1" in the notes. It is this sample which is plotted with filled symbols in Figure 4. It is interesting (though hardly more than suggestive with data of this quality) that the dusty ellipticals—those excluded on the basis that the majority of their 12 μm flux may come from cool dust—appear to have more centrally concentrated 10–12 μm emission than the ones which are not; given that dust is usually seen in optical images in the inner regions of elliptical galaxies this is perhaps not surprising.

We first use the assumed de Vaucouleurs law distribution to calculate the total 12 μm flux density of each elliptical galaxy from the values measured by *IRAS*. This is necessary because although (nearby) elliptical galaxies are extended objects their brightness distributions are strongly centrally peaked and can therefore look like point sources in observations with poor signal to noise ratios observed with relatively low spatial resolution (cf. Rice et al. 1988). The 12 μm flux densities given by Knapp et al. (1989) were found by fitting an assumed point source beam profile to the observed intensity distribution. The *IRAS* beam profile is rectangular and of size 46″ × 270″ at 12 μm. This beam area is of comparable size to the area within r_e, the de Vaucouleurs effect (half-light) radius, for the observed galaxies. Thus, although the galaxies appear to be point sources at this resolution, and any more extended emission would be lost in the noise, the *IRAS* equivalent point source flux density values seriously underestimate the total flux densities for most of the galaxies.

The correction procedure and results are described in detail in Appendix B and were made as follows. We assumed that each galaxy is circular in projection and calculate its effective radius r_e from 2.2 μm aperture photometry if available (cf. Appendix A) or from the optical photometry of Faber et al. (1989) if not. In almost all cases where both 2 μm and optical measurements of r_e are available the agreement is good. The two exceptions are NGC 3377 and NGC 4621, for which the 2 μm and optical determinations differ radically. The geometric mean of the measurements was used for these two objects. The values of r_e are listed in column (9) of Table 2. After calculating the brightness distribution with the appropriate value of r_e we calculated the 12 μm flux density which would have been measured by fitting an assumed point source beam profile to the data. The quantity f_{IRAS} tabulated in column (11) is the fraction of the total flux density registered by the *IRAS* point-source fitting procedure.

The de Vaucouleurs profile is then integrated to form the analogous quantity f_{IRTF}, which is the fraction of the total flux observed in an aperture of radius 2".85, the size used in the 10.2 μm measurements. This quantity is tabulated in column (12). Since it refers to a very small central region, it is quite sensitive to the value of r_e used (it is almost inversely proportional to r_e in the relevant range of r_e). Comparison of the values derived in Appendix A from 2.2 μm photometry and the values obtained by Faber et al. (1989) from optical photometry show that the two independent determinations have an rms difference of about 0.26 in the common logarithm (a factor of 1.8, but cf. Fig. 12 and the discussion in Appendix A), and it is probably reasonable to assign an error of this order to $f_{\rm IRTF}$.

We then color-correct the 12 μm flux density to 10.2 μm using the relation given by Hill et al. (1988) quoted above, and form the observed ratio R corresponding to $f_{\rm IRTF}$:

$$R = \frac{S_{10.2,\rm IRTF} f_{\rm IRAS}}{0.7 S_{12,\rm IRAS}} . \quad (3)$$

As discussed in Appendix B, an error of a factor of 2 in the fitted value of r_e causes an error of up to 30% in the total flux density extrapolated from large aperture measurements like those made by *IRAS*. However, since the signal-to-noise ratio of both the *IRAS* and IRTF observations is small (values of 2 or 3 are typical), the errors in the observed ratio R are dominated by errors in the measurements and are given by

$$\left(\frac{\sigma_R}{R}\right)^2 = \left[\frac{\sigma(S_{\rm IRTF})}{S_{\rm IRTF}}\right]^2 + \left[\frac{\sigma(S_{IRAS})}{S_{IRAS}}\right]^2 \quad (4)$$

Figure 5 shows a plot of the observed ratio of small and large aperture flux densities R (including 2 σ upper limits) versus the predicted ratio $f_{\rm IRTF}$ for the "normal" sample defined above. The errors are very large, but it can be seen that the observed ratios are approximately equal to the calculated ones. This shows that the 10–12 μm emission is spatially distributed like the starlight and therefore probably arises from the stars themselves. There is some tendency for the observed ratios to show a slight excess over the calculated ratios. This may indicate the presence of small amounts of heated dust in the inner regions of many elliptical galaxies or an increased dust to gas ratio in the circumstellar envelopes in the inner regions due to metallicity gradients. This does not contribute significantly to the total 10–12 μm fluxes of these galaxies, however.

Frogel & Whitford (1987) used observations from 2 to 10 μm of the luminosity function and colors of evolved giants in the Galactic bulge to synthesize the expected emission from elliptical galaxies and the bulges of spirals, and found excellent agreement between the observed and calculated colors. They concluded that the mid–infrared ($\sim$10 μm) emission from elliptical galaxies arises from the stars. Our conclusions, based on a quite different approach, confirm this result.

The "abnormal" galaxies are interesting as well. For the strong-nucleus galaxies NGC 1052 and NGC 3998, a considerable fraction of the 12 μm flux is contributed by the inner regions of the galaxy (Fig. 4). These galaxies are both known to have nonthermal radio sources in their nuclei. Becklin, Tokunaga, & Wynn-Williams (1982) observed NGC 1052 at two epochs and found that the 10 μm intensity was constant (while the radio frequency emission was variable) suggesting that the source of the 10 μm emission is not pointlike. It therefore possibly arises from heated dust, perhaps in an accretion disk,

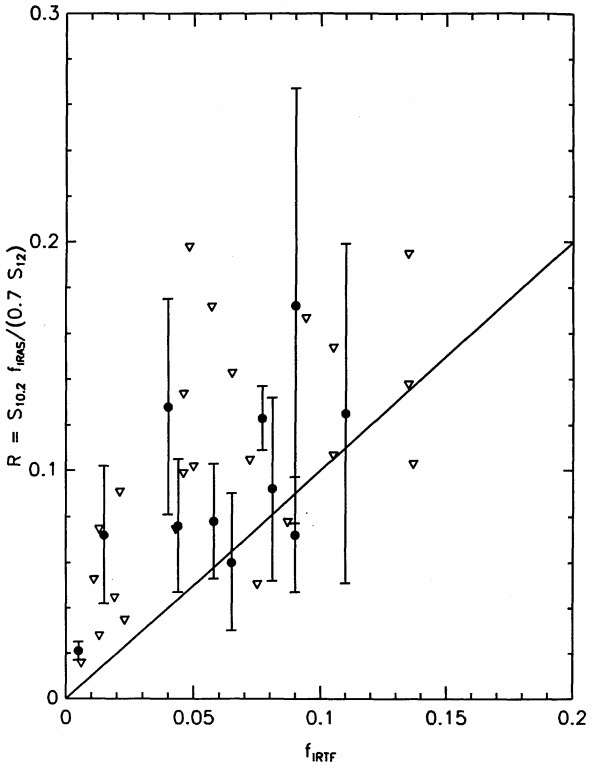

FIG. 5.—Observed fraction of the flux within an aperture of radius 2".85 vs. the ratio calculated for a de Vaucouleurs law for elliptical galaxies. The line represents equality. 2 σ upper limits to the observed ratios are shown. Error bars are shown only for the observed ratios; the calculated values are uncertain by about a factor of 2 because of uncertainties in the effective radii (see text).

in the vicinity of the central engine. NGC 3998 is a possible new source of this type. It is of some interest in this context that NGC 4278, an elliptical galaxy with an active nucleus whose properties are very similar to those of NGC 1052, apparently does not have such a source (Tables 1 and 2).

Since we have established to our satisfaction that the 12 μm emission from normal elliptical galaxies is distributed like the starlight, we proceed in the next section to model the emission, to see how much of it is photospheric and how much circumstellar, and to use the results to examine both the nature of the highly evolved stellar population in elliptical galaxies and the injection rate of dust.

5. THE EVOLVED STELLAR POPULATION AND DUST INJECTION RATE FOR ELLIPTICAL GALAXIES

We investigate this question by comparing the 2.2–12 μm colors of elliptical galaxies with those of evolved stars in the local region of the Galaxy, in the Galactic bulge, and in the bulge of M31. There are many uncertainties in this procedure: (*a*) the 12 μm flux densities in even the brightest ellipticals are small and are measured at the level of only a few times the rms noise with, in addition, some small uncertainties due to calibration and large uncertainties due to the definition of the baseline (cf. Knapp et al. 1989): (*b*) the observed 12 μm flux densities need to be corrected to the total flux density for each galaxy, and this procedure carries significant uncertainties cf. § 4): (*c*) the 2.2 μm emission is extended, and total flux densities are only available from large aperture measurments. Since the

12 μm and 2.2 μm flux densities cannot be directly compared, we proceed as follows. We take the available 2.2 μm data (compiled from the tabulation by Gezari, Schmitz, & Mead 1987) measured through apertures of several diameters and fit a de Vaucouleurs law profile to the data. The resulting value of r_e is then used to calculate the effective circular aperture which corresponds to the dimensions of the *IRAS* 12 μm beam (see Appendix B and Table 4) and to calculate the 2.2 μm flux within the aperture. The 2.2 μm flux and the observed *IRAS* 12 μm flux density then give the mean 2.2–12 μm color within the effective *IRAS* beam diameter. This procedure is formally equivalent to comparing the extrapolated total fluxes for both the *IRAS* and 2.2 μm data, but this description has several transparent advantages: first, the effective beam diameter is very insensitive to the value chosen for r_e (cf. Table 4), so the typical errors in r_e of factors of two have very small effects on the colors. Second, the effective apertures are generally in the range of the apertures used for the 2.2 μm measurements, so the resulting 2.2 μm flux almost always results from an interpolation in the multiaperture data rather than an extrapolation. Third, the colors refer to the regions of the measurements themselves, not to an extrapolation to some total flux.

We selected galaxies of types E and E/S0 from the tabulation of Knapp et al. (1989) for which sufficient 2.2 μm multiaperture photometry exists to determine an effective radius according to the following criteria: (a) galaxies detected at greater than the 3 σ level at 12 μm for which S_{12}/S_{100} is greater than twice the typical value (0.042) for spiral galaxies (cf § 2, Fig. 1 and § 4). If there is no 100 μm detection, the 1 σ upper limit is taken. This caveat makes us reasonably sure that the 12 μm flux density is not dominated by emission from interstellar dust. We use a 12 μm flux density corrected for emission from cool dust by subtracting 0.042 times either the 100 μm flux or its 1 σ limit. As was discussed in § 3, the corrections for galaxies with 100 μm upper limits are in general very small. This is the $S_{12,c}$ entry in column (4) of Table 2. (*b*) galaxies with upper limits at 12 μm (i.e. those for which the 12 μm flux density is $\leq 3\,\sigma$).

NGC 1052 and NGC 3998 were removed from the sample because the 12 μm flux densities are dominated by the central bright infrared source (Fig. 4). The resulting sample is identified in the notes to Table 2 as "sample 2." It contains 35 galaxies with 12 μm detections and 46 with upper limits.

The results are plotted in Figure 6, in which the *IRAS* flux density at 12 μm is plotted against the flux density at 2.2 μm within the *IRAS* effective aperture; the upper limits at 12 μm are 2 σ. (Note that the 2.2 μm flux plotted is obtained from the extrapolated total flux tabulated in Table 2 by multiplying by f_{IRAS}, thus effectively undoing the extrapolation.) The vertical error bars have been arbitrarily lengthened by 30% to attempt to allow for errors associated with errors in r_e, the assumption of circular symmetry, the *IRAS* baseline, and other problems.

It is seen that the 12 and 2.2 μm flux densities are roughly correlated and that the 12 μm upper limits are largely nonrestrictive, i.e., do not suggest the presence of the separate population of galaxies with low 12 μm flux densities (we examine this more carefully below). It is clear that the 2.2 μm data set, while heterogeneous and incomplete, goes fainter than the *IRAS* data, and most of the 12 μm upper limits belong to galaxies for which the 2.2 μm flux is less than about 500 mJy. For galaxies brighter than this at 2.2 μm, which contains roughly half the detected sample, the 12 μm upper limits have essentially no effect on the statistics, and the upper limits at

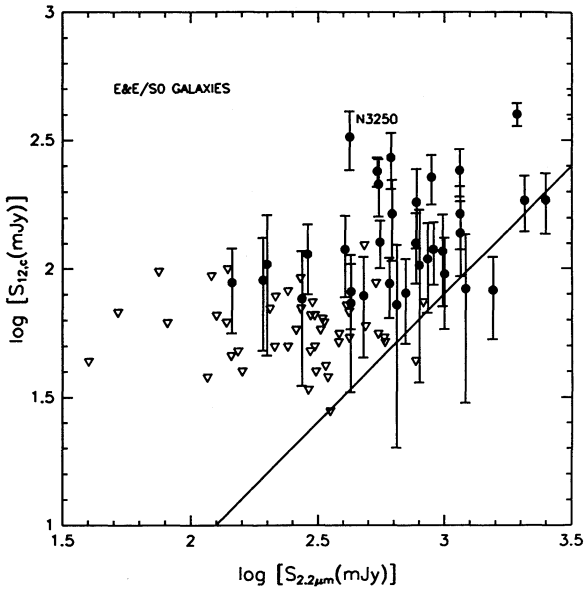

FIG. 6.—12 μm flux density corrected for the contribution of cool interstellar dust for elliptical galaxies vs. 2.2 μm flux density contained within the *IRAS* 12 μm aperture. Galaxies detected at $\geq 3\,\sigma$ at 12 μm are indicated by the dots; for those not detected, 2 σ upper limits are given by the triangles. The solid line shows the relationship for evolved cool giant stars with no mass loss (cf. Fig. 7).

fainter levels are quite consistent with the bright galaxy data and a statistical proportionality between the 2.2 and 12 μm flux densities. We will see below that the luminosities at 2.2 and 12 μm are very well correlated and are proportional to each other, so the distribution of 12 μm fluxes at a given 2.2 μm flux should not depend on the 2.2 μm flux level.

The linear correlation coefficient for the data for the 35 detected galaxies is 0.86, and the slope of the relationship is $S_{12,c} = (0.138 \pm 0.014)\, S_{2.2,\mu m}$, where $S_{12,c}$ is the 12 μm emission corrected for interstellar dust. We calculate only the slope in the S_{12} versus $S_{2.2}$ relationship rather than attempting any more sophisticated analysis because of the large errors and uncertainties. Also plotted in Figure 6 is the relation $S_{12} = 0.08 S_{2.2}$, typical of the photospheric emission from K and M giant stars (see below). The scatter in the galaxy data, if real, is of considerable interest if, as we will suggest, the excess emission comes from circumstellar envelopes. Some high 12 μm fluxes with relatively small errors are probably associated with confusion with later type galaxies or with nuclear sources, though NGC 3250, which has a very large 12 μm flux density and is the most discrepant point in Figure 6, has an IRTF 10.2 μm upper limit which does not suggest the presence of a nuclear source, nor is there another comparable bright galaxy nearby. Its image on the Palomar Sky Survey print, however, is not at all smooth and does not look to our eyes like that of an elliptical galaxy. Whether or not it is included in the analysis makes essentially no difference; the slope is affected less than 1%.

We subjected these data to a few simple analyses to look into the question of variability of the ratio and the effects of the upper limits. As one might expect, the coefficient in the $S_{12,c}$ to $S_{2.2}$ relationship drops as one moves the lower limit of the 2.2 μm fluxes considered to larger values, thereby removing upper limits from the sample. If one considers only 2.2 μm fluxes greater than 300 mJy, the sample size drops to 30, there are 22

of the original 46 upper limits, and the coefficient becomes 0.137 ± 0.014, insignificantly different from that for the full sample. At a limit of 600 mJy, the sample is 22 galaxies, only two upper limits survive, and the coefficient is 0.128 ± 0.012. At 800 mJy, there are no upper limits, and the coefficient is 0.122 ± 0.013. For this sample, the correlation coefficient is 0.93, and it progresses steadily from 0.86 to this value as the 2.2 μm lower flux limit is increased. The formal values of χ^2 about the linear fit are large for all of these samples, about 3 times the sample size; it is quite possible, however, that we have seriously underestimated the errors in the *IRAS* photometry (the errors in the 2.2 μm photometry should be negligible) from the baseline fitting, and a doubling of the original quoted errors, which would be required to bring the value of χ^2 to reasonable consistency with a unique $S_{12,c}$–$S_{2.2}$ relationship seems by no means out of the question. Add to this the possibilities of misclassification and confusion, and it is clear that much better data and a much more careful treatment is required to settle the question of whether there is cosmic variability in the relation. We proceed as if there were little or no variation, and adopt a value of 0.13 for the ratio of the 12 and 2.2 μm flux densities for all elliptical galaxies.

We now compare the mean 12/2.2 μm color for elliptical galaxies with the corresponding colors for evolved red giant stars in the Galaxy. We have taken this approach rather than using observations of Galactic bulge stars (e.g., Frogel & Whitford 1987) because, although the properties of the bulge giants probably more closely resemble those of stars in elliptical galaxies, we can directly observe and measure mass loss for the nearby giants. We shall use these observations to estimate how much of the 12 μm emission from elliptical galaxies is due to circumstellar material and to estimate the rate of mass return from the ensemble of evolved stars. Figure 7 shows the relationship between the 12 and 2.2 μm flux densities for two samples of K and M giants. The first sample contains nearby bright K and *M* giant stars and is given by Judge (1989). The second is a sample of high-latitude evolved stars selected from the *IRAS* all sky survey (see Knapp, Rauch, & Wilcots 1990). Both samples show that most of the stars have $S_{12\,\mu m}/S_{2.2\,\mu m} = 0.08$, corresponding to K and early M giants with effective temperatures about 4500 K and with no circumstellar material. This relationship is plotted with a solid line in Figure 6. Some few stars in both of these samples have 12 μm flux densities well in excess of this relationship, and many of these stars are known from molecular line measurements to be losing considerable amounts of mass. The mean ratio of 12 and 2.2 μm flux densities in the elliptical galaxies is 0.13, significantly greater than the value for K and early M giant stars. Since we have removed galaxies with known strong nuclei and have corrected for the contribution of interstellar dust, we believe that this demonstrates the presence of a population of stars which is losing mass.

Stellar populations in elliptical galaxies are usually considered closely to resemble those in Galactic bulges. Much recent beautiful work has been done on this problem in the near infrared regions (1–2 μm) of the spectrum and has shown that this spectral region is dominated by late-type giants from a metal-rich population such as that observed in the bulge of the Galaxy (Frogel & Whitford 1987; Rich 1988; Frogel 1990; Terndrup, Fogel, & Whitford 1990; Frogel et al. 1990). Here, we compare the integrated light of ellipticals with that from the bulge of M31. Soifer et al. (1986) mapped the bulge of M31 at 12 μm using the *IRAS* data. There are no *K* band observations on scales of several arcminutes for the bulge of M31, but Aaronson, Mould, & Huchra (1980) mapped it at 1.6 μm. Within an aperture of diameter 4′ centered on the nucleus of M31 the H (1.6 μm) magnitude is 2.95. Persson et al. (1980) find $H - K = 0.24$ for the bulge of M31, so that the corresponding *K* magnitude is 2.71, giving a flux density of 50.9 Jy. The *IRAS* 12 μm flux density within the same aperture is 4.94 Jy, giving $S_{12}/S_{2.2} = 0.10$. This is higher than the corresponding value for Galactic K and M giants, but is less than the mean found for elliptical galaxies.

Figure 8 shows the plot of L_{12} versus $L_{2.2}$ for the elliptical galaxies detected at 12 μm. As Figure 6 shows, the upper limits

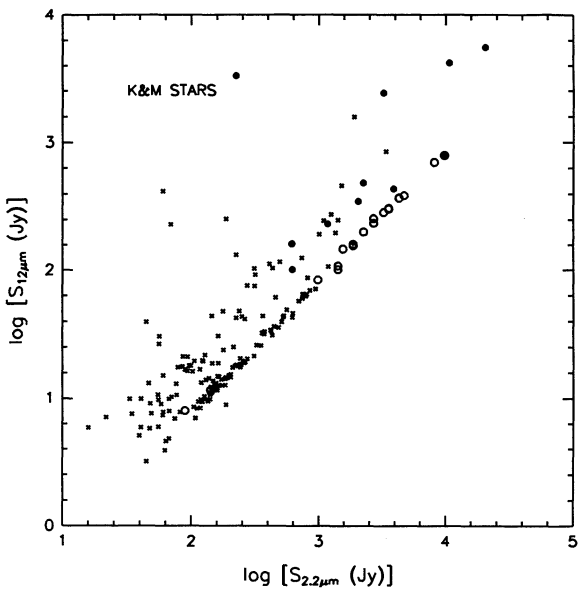

FIG. 7.—12 μm flux densities for two samples of evolved stars: (1) the sample of K and M giants of Judge (1989). Filled symbols correspond to stars known from molecular line observations to be losing mass. (2) The sample of high-latitude stars from Knapp et al. (1990) (*crosses*).

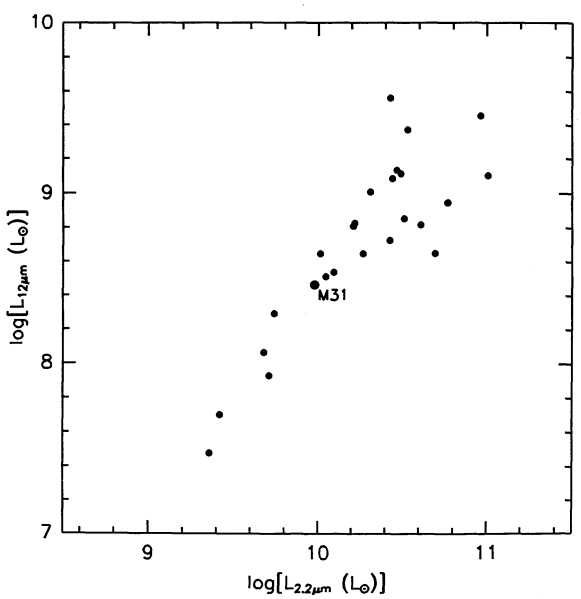

FIG. 8.—12 μm vs. 2.2 μm luminosity for elliptical galaxies. The large filled circle represents the data for M31.

for the nondetected galaxies are mostly nonrestrictive, so that we are not making any serious error by ignoring these data points. Corrected asymptotic magnitudes are used, and the data for the bulge of M31 are included (cf. Appendix B). The distances were estimated from the redshifts and a Hubble parameter of 100 km s^{-1} Mpc^{-1}. There is a large amount of scatter in this plot, but the best fit straight line has a power-law slope of 1.0 ± 0.1, i.e., L_{12}/L_2 is constant. It is tempting to speculate that the slope steepens a little for the low luminosities, as one might expect, since the giant branch is hotter for these lower metallicity objects and the dust-to-gas ratio should be lower in the outflows, but one clearly needs much better data before anything useful can be said.

The excess 12 μm flux density for elliptical galaxies can now be used to measure the total rate of mass loss. This has been done by several authors (e.g., Soifer et al. 1986, Jura 1986; Jura et al. 1987; Frogel & Whitford 1987) using data at wavelengths between about 1 and 10 μm. These calculations are made by assuming that the evolved stars are blackbodies at infrared wavelengths, measuring the excess 10 μm emission over that expected for a blackbody, calculating the mass of circumstellar dust and assuming some value of the gas to dust ratio. Frogel & Whitford (1987) use the giant luminosity function measured for the Galactic bulge and photometry of Galactic bulge giants, and show that much of the infrared excess is due to middle M stars. In this paper, we take a different and more empirical approach: we estimate the 12/2 μm ratio for giants known not to be losing mass, and use these colors to estimate the 12 μm excess for elliptical galaxies and for mass losing stars. Molecular line observations of the latter give the mass-loss rate, so that the infrared excess can be directly used to measure the mass loss by using the calibration provided by these observations.

We selected a small sample of oxygen-rich evolved stars from which CO emission has been detected and which lie at high Galactic latitudes ($|b| > 60°$)—these stars are likely to belong to the old disk population and may be a reasonably close match to the $\sim 1\ M_\odot$ metal-rich stars currently evolving through the red giant phases in elliptical galaxies. We estimated distances for all of these stars by assuming the absolute K magnitude of $M_k = -8.1$ mag, corresponding to $L_{\rm bol} = 5000\ L_\odot$ (cf. the data discussed by Frogel 1990) and correcting the 12 μm flux density for photospheric emission by assuming S_{12}(photospheric) $= 0.08\ S_{2.2}$, as found above for non–mass-losing stars. The mass-loss rates for these stars are given in Table 3. Figure 9 shows the very tight correspondence between $S_{12,\rm CS}$, the excess 12 μm luminosity, and the mass-loss rate, with

$$\dot{M} = 1.6 \times 10^{-5} \left(\frac{D}{\rm Mpc}\right)^2 \left(\frac{S_{12,\rm CS}}{\rm mJy}\right) M_\odot\ {\rm yr}^{-1}\ . \qquad (5)$$

For elliptical galaxies, $S_{12}/S_{2.2} = 0.13$, so that about 38% for the 12 μm light is likely due to the circumstellar shells produced by mass loss. When the 12 μm flux density is corrected for contamination by interstellar dust using the relationship found for spiral galaxies in § 2, we have:

$$\dot{M} = 6 \times 10^{-6} \left(\frac{D}{\rm Mpc}\right)^2 \left(\frac{S_{12} - 0.042 S_{100}}{\rm mJy}\right) M_\odot\ {\rm yr}^{-1}\ . \qquad (6)$$

These estimates are similar to those found by previous authors (e.g., Jura et al. 1987; Frogel & Whitford 1987). For high-luminosity elliptical galaxies like NGC 4472, equation (6) gives $\dot{M} = 0.7\ M_\odot\ {\rm yr}^{-1}$.

As discussed above, $L_{12}/L_{2.2} \sim 0.13$ is roughly constant for elliptical galaxies i.e., the 2.2 μm luminosity directly measures the population of evolved stars which are losing mass, and the data given in Figure 8 give an estimate of the mass-loss rate from the 2.2 μm luminosity of

$$\dot{M} = 8 \times 10^{-7} \left(\frac{D}{\rm Mpc}\right)^2 \left(\frac{S_{2.2}}{\rm mJy}\right) M_\odot\ {\rm yr}^{-1} \qquad (7a)$$

or

$$\dot{M} = 0.0021[L_{2.2}/(10^9\ L_\odot)]\ M_\odot \qquad (7b)$$

where we have taken the absolute K magnitude of the sun to be 3.40 and the K flux density at 0.0 mag to be 618 Jy (Johnson 1966; Selby et al. 1980).

This estimate is similar to previous values based on the optical luminosity and semi-empirical notions about total mass loss in the later evolutionary stages of low-mass stars. Faber & Gallagher (1976) find that $\dot{M} = 0.015[L_B/(10^9\ L_\odot)]$ for objects with colors and star-formation histories appropriate to large elliptical galaxies. The $B - K$ color of big ellipticals is about 4.0 and that of the Sun 2.1, so their coefficient translated into the K luminosity is 0.0026, in entirely fortuitous agreement with our results. It is to be stressed, however, that the two estimates are completely independent.

TABLE 3

MASS-LOSS RATES FOR NEARBY GALACTIC OLD DISK POPULATION STARS

Star	S_{12}(Jy)	D(pc)	$\dot{M}(M_\odot\ {\rm yr}^{-1})$	References
Y UMa	112	330	1.3×10^{-7}	1, 2
X Her	302	220	2.6×10^{-7}	3, 4
g Her	102	160	5.6×10^{-8}	3, 4
TX Cam	1594	440	4.5×10^{-6}	4, 5
RS Cnc	256	200	1.5×10^{-7}	5
Y Lyn	45	340	1.1×10^{-7}	4
BK Vir	136	280	1.0×10^{-7}	2
RT Vir	341	270	3.3×10^{-7}	5, 6
SW Vir	436	190	2.5×10^{-7}	1, 3, 4
RX Boo	610	195	6.1×10^{-7}	5

NOTES.—Values of S_{12} are corrected for photospheric emission. Mass-loss rates calculated for CO(1–0) and CO(2–1) observations from the papers listed below.

REFERENCES.—(1) Knapp 1992; (2) Zuckerman & Dyck 1989; (3) Zuckerman & Dyck 1986a; (4) Wannier & Sahai 1986; (5) Knapp & Morris 1985; (6) Zuckerman & Dyck 1986b.

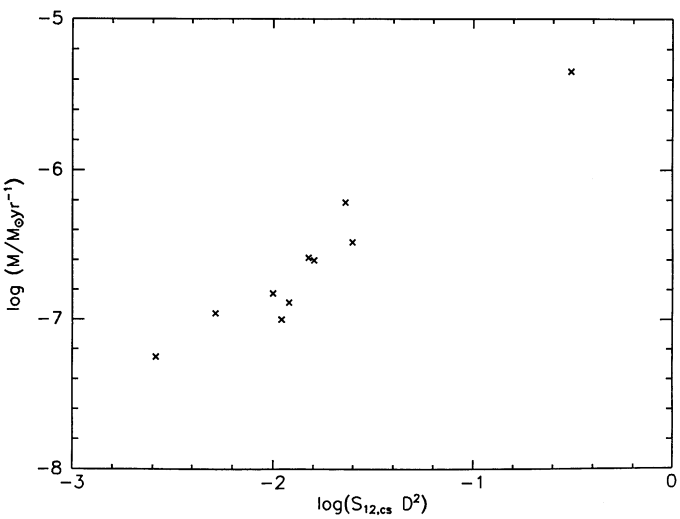

FIG. 9.—Mass-loss rate $\dot{M}$ in $M_\odot\ {\rm yr}^{-1}$ for galactic old disk stars vs. 12 μm luminosity $S_{12,\rm CS} D^2$, where $S_{12,\rm CS}$ is the 12 μm flux density corrected for photospheric emission, in mJy, and D is the distance in Mpc.

The optical–infrared colors of elliptical galaxies depend on the metallicity and luminosity (mostly through metallicity, but perhaps also through differences in star-formation history) of the galaxy (the B and K band data discussed in Appendix A, for example, clearly show the $B - K$ color–luminosity dependence for elliptical galaxies), and the K-band data much more nearly measure the light of the mass-losing population; indeed, we see little deviation from linearity in our 2.2–12 μm luminosity ratio of galaxies of widely differing luminosities. The K band luminosity should therefore give a better estimate for the global mass-loss rate in an elliptical galaxy than does the optical luminosity.

6. CONCLUSIONS

In this paper, we discuss the origin of the 12 μm emission seen by *IRAS* from bright nearby elliptical galaxies. Several possible sources for the 12 μm emission are considered, including small interstellar dust grains, larger dust grains heated to higher temperatures than in spiral galaxies by X-ray photons, hot dust near active Galactic nuclei, and the photospheres and circumstellar dust shells of evolved cool red giant stars. We find the following:

1. The 12 μm emission from elliptical galaxies is well in excess of the value expected for interstellar dust except for a few very dusty elliptical galaxies like NGC 3928 and NGC 5128.

2. Examination of a mean 60/100 μm ratio for elliptical galaxies shows that it is typically smaller than that for spiral galaxies, suggesting that the dust in elliptical galaxies is, if anything, cooler than it is in spiral galaxies. It is therefore unlikely that the 12 μm emission is due to hot interstellar dust in elliptical galaxies.

3. A sample of nearby 12 μm–bright elliptical galaxies was observed at the adjacent wavelength of 10.2 μm through small apertures using the IRTF. These observations were made to check the possibility that the 12 μm emission is due, directly or indirectly, to the presence of an active galactic nucleus. Together with the observations of Papers I and II, these data show that for almost all normal elliptical galaxies the 12 μm emission is extended on the scale of the galaxy and does not originate in an active nucleus.

4. A few exceptions to the above were found. Significant numbers of the radio galaxies observed in Paper II have most of their 10–12 μm emission from a compact central source, as do the nearby E/S0 galaxies NGC 1052 and NGC 3998 which both contain nuclear radio sources. The nuclear infrared emission is probably due to dust heated by the active galactic nucleus.

5. Quantitative comparison of the observations with the de Vaucouleurs surface brightness distribution shows that the 12 μm emission from normal elliptical galaxies is distributed like the starlight and therefore is likely due to photospheric and circumstellar emission from evolved red giant stars in the galaxies.

6. The contributions of emission from the photospheres and from circumstellar dust are evaluated by comparing the 12 and 2.2 μm flux densities for elliptical galaxies with the values found for evolved Galactic red giant stars with and without circumstellar envelopes. The colors were found using the equivalent 2.2 μm flux density inside the *IRAS* 12 μm beam, calculated assuming a de Vaucouleurs law for the Galactic surface brightness distribution. The mean 12/2.2 μm color for elliptical galaxies is significantly redder than that for Galactic K and early M giants and shows that about 40% of the 12 μm emission is circumstellar in origin. The resulting values of the global mass-loss rate from evolved stars in elliptical galaxies agree well with values found from the optical flux densities and quite different physical considerations.

We are very grateful to the IRTF staff, especially Charlie Kaminski, for their support of the observations. We also thank Jay Frogel and Chas Beichman for many useful comments. The Infrared Telescope Facility is operated by the University of Hawaii under contract from the National Aeronautics and Space Administration. This research was partially supported by the National Science Foundation via grants AST 86-15684 to the University of Hawaii and AST 89-21700 to Princeton University, by NASA under the *IRAS* Extended Mission Project via grants R010-87 to U.C.L.A. and NAG5-1226 to Princeton University, and by the United Airlines Frequent Flyer program.

APPENDIX A

2.2 μm TOTAL FLUXES AND EFFECTIVE RADII FOR ELLIPTICAL GALAXIES

Comparing the 12 μm *IRAS* fluxes with 2.2 μm fluxes in order to investigate the mass loss requires that both sets of fluxes refer to the same area, since elliptical galaxies are extended sources. In this Appendix we consider the problem for the 2.2 μm fluxes; the rather more complex question of the 12 μm *IRAS* fluxes with that instrument's complex spatial response will be discussed in Appendix B.

Elliptical galaxies are well-known to be described with good accuracy by the surface-brightness distribution of de Vaucouleurs (1946) (eq. [2]). That relation has only two parameters, a characteristic radius r_e containing half the projected flux, and a surface brightness at that radius, or, equivalently, a total flux. Good effective radii have been determined for many ellipticals from multiaperture photoelectric measurements by Faber et al. (1989) in the B band; elliptical galaxies, however, are known in many cases to have quite strong color gradients, and we felt it better to try to determine effective radii when we could directly from the 2.2 μm data.

Extensive multiaperture photometry of elliptical galaxies has been carried out at 2.2 μm by a large number of authors and groups. The data used here were gathered from the enormously useful compilation by Gezari et al. (1987) and are taken from photometry from the following papers: Becklin et al. (1971); Penston (1973); Grasdalen (1975); Frogel et al. (1975); Grasdalen & Joyce (1976); Glass (1976); Frogel et al. (1978); Persson et al. (1979); McAlary, McLaren, & Crabtree (1979); Mould (1981); Walsh & White (1982); Griersmith, Hyland, & Jones (1982); Jones & Hyland (1982); Rieke, Lebofsky, & Kemp (1982); Becklin et al. (1982); Axon, Bailey, & Hough (1982); Longmore & Sharples (1982); Impey (1983); Adams, Adamson, & Giles (1983); Glass (1984); Lépine, Braz, & Epchtein (1984); Glass & Moorwood (1985); Cutri & McAlary (1985); Willner et al. (1985); Price (1985); Paper I; Sparks et al. (1986); and Killeen, Bicknell, & Carter (1986).

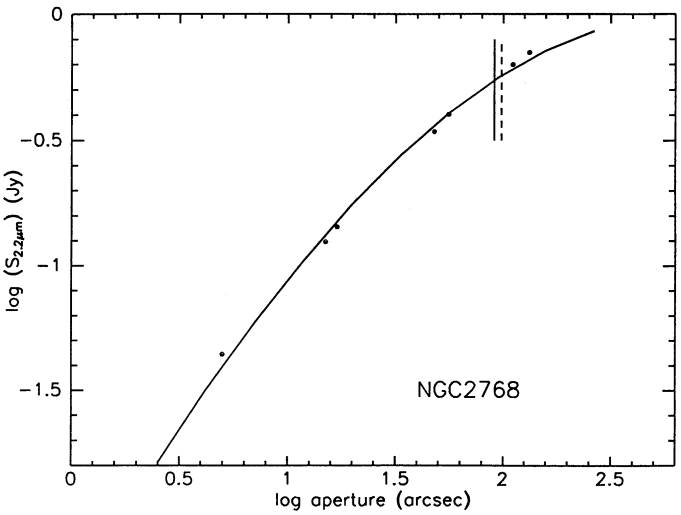

FIG. 10a

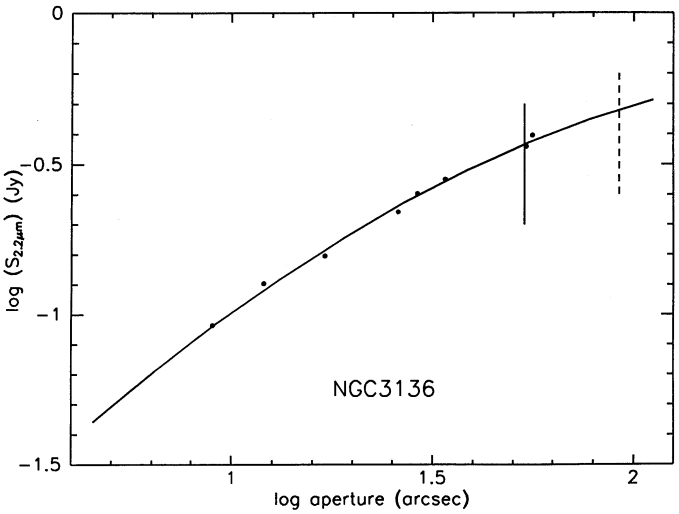

FIG. 10b

FIG. 10.—2.2 μm flux density vs. aperture for the elliptical galaxies (*a*) NGC 2768 and (*b*) NGC 3136. The curve is a de Vaucouleurs law profile fitted to the aperture data. The solid vertical line is at twice the de Vaucouleurs effective radius, and the dashed line at the 12 μm *IRAS* effective aperture.

It is possible to derive an effective radius from measurements with only two apertures, since the ratio of the contained flux at some radius to that at a larger one is a monotonically increasing function of the assumed r_e. One would like more measurements, of course, to get some feeling for the consistency of the photometry and the quality of the fit to the de Vaucouleurs model, and most of the galaxies in our sample have photometry with three or more apertures.

We have found effective radii by simple least-squares fits in the logarithm of the cumulative flux, assuming circular symmetry. This assumption has been made throughout the work in this paper, both here and for the *IRAS* reductions; it would be essentially harmless if the *IRAS* data were taken through circular apertures as well, but this is not the case, and the procedure introduces real uncertainties, which, however, are masked by the poor signal-to-noise ratios of the presently available data. The effective radii derived are, in general, within the range of radii for which there are measurements. The total fluxes come from these fits as well. It is to be stressed that the flux within the quoted effective radius is in almost all cases a measured (interpolated) quantity, and the total flux is simply twice that, but in very few cases is the profile measured and seen to be accurately de Vaucouleurs for radii significantly larger than r_e.

Two examples of the fitted cumulative de Vaucouleurs law profiles are shown in Figure 10.

Figure 11 shows the calculated total 2.2 μm flux density plotted versus the total asymptotic blue magnitude B_T^0 from Faber et al. (1989). The blue magnitudes are corrected for Galactic extinction; the 2.2 μm flux densities are not, but the corrections would be very small. Figure 12 shows a histogram of the logarithm of the ratio of our 2.2 μm–derived effective radii to the optical ones from

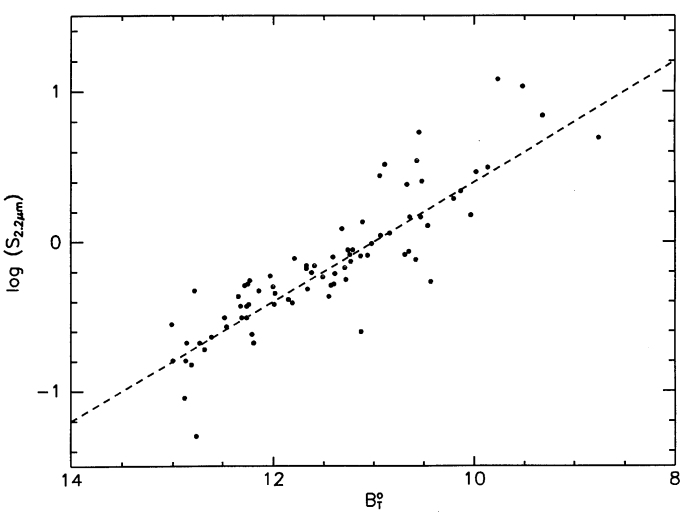

FIG. 11

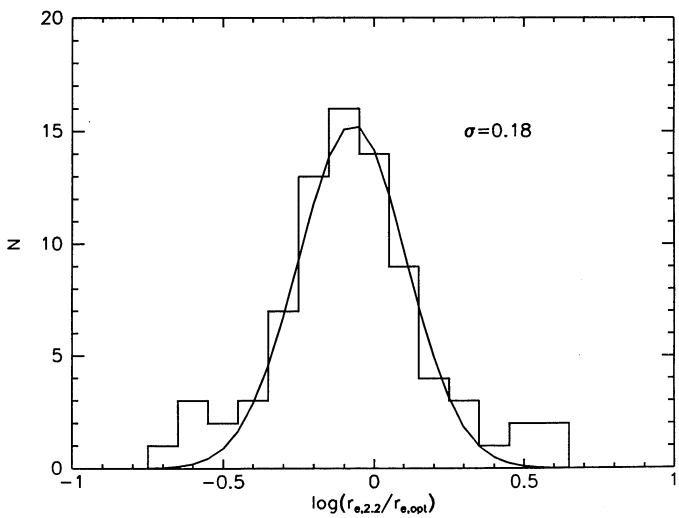

FIG. 12

FIG. 11.—Total asymptotic flux density at *K* band (2.2 μm) vs. asymptotic blue magnitude (B_T^0) from Faber et al. (1989) for elliptical galaxies. The dotted line corresponds to a constant $B - K$ color of 4.00.

FIG. 12.—Histogram of the log of the ratio of the effective radii obtained from 2.2 μm photometry to the values obtained in *B* by Faber et al. (1989). The curve is a Gaussian of standard deviation 0.18 and total weight 93% of the sample of 80. The mean ratio is −0.07, corresponding to the 2.2 μm effective radii a factor of 1.2 smaller than the *B* ones.

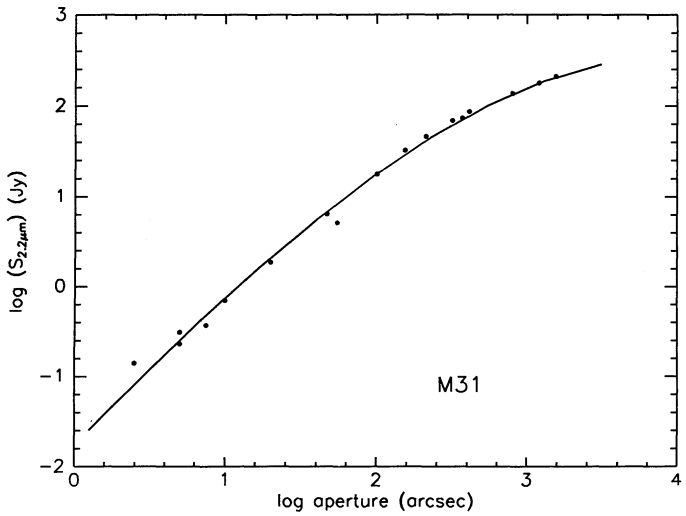

FIG. 13.—2.2 μm flux density vs. aperture for M31. The curve is a de Vaucouleurs law profile fitted to the aperture data.

Faber et al. (1989) for those galaxies for which both are available. The formal standard deviation in the logarithm is 0.26, or a factor of 1.8, though most of this comes from a few highly discrepant points and the main part of the histogram is better fit by a Gaussian with a standard deviation of about 0.18 (a factor of 1.5) which contains about 93% of the points. The mean is shifted by 0.07, or a factor of about 1.2, in the expected sense that the r_es derived from the 2.2 μm data are smaller; i.e., the infrared light is more concentrated than the blue.

These effective radii and total 2.2 μm fluxes are tabulated in Table 2 for all the galaxies for which enough 2.2 μm data exist for the determination. The fluxes have been determined from the K magnitudes by assuming that the 2.2 μm flux density of Vega ($K = 0.0$) is 618 Jy (Johnson 1966; Selby et al. 1980). For those galaxies which have 10.2 μm measurements but not 2.2 μm data, we have used the r_e values from Faber et al. (1989). For two galaxies in sample 1 the optical and 2.2 μm radii were so discrepant that we used geometric means of the two values; those galaxies are NGC 3377, with 33".7 and 6".6 for the blue and K values, respectively, and NGC 4621, with 46".3 and 16".2. The comparisons made in § 5 involving the 2.2 and 12 μm fluxes are so insensitive to the value of r_e used that we used the 2.2 μm value no matter how discrepant it is.

We also calculated the asymptotic K band flux density for the bulge of M31. K band photometry in apertures between 2".5 and 55" has been done by Sandage, Becklin, & Neugebauer (1969), Persson et al. (1980) and Martinez-Roger, Phillips, & Sanchez-Magro (1986). Aaronson et al. (1980) mapped M31 in the H band (1.6 μm) in apertures between 101" and 1554". These H magnitudes were used to estimate K magnitudes using the $H - K$ color of 0.24 measured by Persson et al. (1980). Figure 13 shows the cumulative 2.2 μm flux density of the M31 bulge. The data are well fit by a de Vaucouleurs law profile with an effective radius of 782" and a total K band flux density of 416 Jy ($K = 0.43$).

APPENDIX B

THE RELATIONSHIP OF THE *IRAS* 12 μm FLUX DENSITY TO THE TOTAL FLUX DENSITY: THE *IRAS* EFFECTIVE APERTURE AND f_{IRAS}

The *IRAS* beam at 12 μm is roughly rectangular in the cross-scan direction with a length of about 270" and approximately gaussian in the in-scan direction with a full width at half-maximum of about 46", though there are small variations from detector to detector (see the *IRAS* Explanatory Supplement 1988, pp. IV3–8 and V14). The *IRAS* point-source fluxes are found by fitting this response function at a given position and adding the results for all scans whose centers pass sufficiently near that position. The result for extended objects is that the fluxes found are smaller than the real ones, since some of the flux appears in the wings of the peak and is not properly weighted by the beam shape.

We have calculated the corrections for round de Vaucouleurs galaxies by convolving de Vaucouleurs profiles of various effective radii with the idealized rectangular Gaussian described above and then fitting the same Gaussian to the resulting profile, thus mimicking the observations and reductions leading to the *IRAS* fluxes. Since the galaxies in this study typically have many *IRAS* scans at quite disparate directions the data for which are summed to obtain the quoted fluxes, the fact that the galaxies are, in fact, not round, probably does not introduce any serious errors. If there were only one scan, any E5 galaxy with a mean effective radius of 50", typical for our sample, could have an error in the derived flux of up to about 30%, but two scans at right angles would have a maximum error from this source of only about 1%; in general, we expect errors of the order of 10% or less, in nearly all cases small compared to the other noise sources.

The correction factor is most conveniently expressed as the quantity $f_{\rm IRAS}$, which is the fraction of the total flux found by the *IRAS* fitting procedure; it is tabulated as a function of the effective radius in Table 4, column (3). Another useful notion is the diameter of a round aperture which contains the same fraction of the total flux, $A_{\rm eff,IRAS}$, which is tabulated in column (4). In comparing *IRAS*

TABLE 4

FRACTIONAL FLUXES FOR THE IRTF AND *IRAS* BEAMS AND *IRAS* EFFECTIVE APERTURES FOR THE DE VAUCOULEURS LAWS

r_e (1)	f_{IRTF} (2)	f_{IRAS} (3)	$A_{eff,IRAS}$ (4)
2″.0	0.597	0.9815	57.84
3.0	0.483	0.9657	63.98
5.0	0.351	0.9307	71.16
7.0	0.273	0.8958	75.70
10.0	0.203	0.8469	80.40
14.0	0.149	0.7892	84.72
20.0	0.105	0.7168	89.14
30.0	0.0678	0.6237	93.96
50.0	0.0374	0.4983	99.70
70.0	0.0285	0.4165	103.24
100.0	0.0154	0.3348	106.80
140.0	0.00981	0.2653	109.96
200.0	0.00598	0.2016	113.10
300.0	0.00329	0.1426	116.42
500.0	0.00152	0.0877	120.20
700.0	0.000897	0.0618	122.46
1000.0	0.000510	0.0417	124.68

data with conventional aperture photometry, it is the radius which is some sense best approximates what *IRAS* sees, and we make use of this in the analysis in § 5. It is seen from Table 4 that the effective aperture is a very slowly varying function of the effective radius, changing by only about a factor of 2 as r_e varies by a factor of 500, from 2″ to 1000″. Thus if one wishes to compare aperture photometry at one wavelength with *IRAS* photometry at another, even large errors in the assumed r_e have very little effect if the comparison is made at the effective aperture. This can be done with high accuracy if aperture data are available at radii larger and smaller than the *IRAS* effective aperture size, which is the case for most of the 2.2 μm photometry used in this paper. For effective radii in the range of interest in this paper, errors of even a factor of 5 in r_e give rise to errors of only about 20% in the effective apertures and comparable errors in the fluxes.

We also tabulate in Table 4 the corresponding but much simpler quantity f_{IRTF}, the fraction of the total flux observed in the IRTF 5″.7 aperture, which is calculated simply by integrating the de Vaucouleurs profile to the appropriate radius.

REFERENCES

Aaronson, M., Mould, J., & Huchra, J. P. 1980, ApJ, 237, 655
Aaronson, M., Persson, S. E., & Frogel, J. A. 1981, ApJ, 245, 18
Adams, D. J., Adamson, A. J., & Giles, A. B. 1983, MNRAS, 202, 241
Axon, D. J., Bailey, J., & Hough, J. H. 1982, Nature, 299, 234
Becklin, E. E., Frogel, J. A., Kleinman, D. E., Neugebauer, G., Ney, E. P., & Strecker, D. W. 1971, ApJ, 170, L15
Becklin , E. E., Tokunaga, A. T., & Wynn-Williams, C. G. 1982, ApJ, 263, 624
Bertola, F. 1987, in IAU Symp. 127, Structure and Dynamics of Elliptical Galaxies, ed. T. de Zeeuw (Dordrecht: Reidel), 135
Boulanger, F., Beichman, C., Désert, F. X., Helou, G., Pérault, M., & Ryter, C. 1988, ApJ, 332, 328
Canizares, C. R., Fabbiano, G., & Trinchieri, G. 1987, ApJ, 312, 503
Cutri, R., & McAlary, C. W. 1985, ApJ, 296, 90
de Jong, T., et al. 1984, ApJ, 278, L67
de Vaucouleurs, G. 1948, Ann. d'Astrophys., 11, 247
Draine, B. T. 1990, in The Interstellar Medium in Galaxies, ed. H. A. Thronson & J. M. Shull (Dordrecht: Kluwer), 483
Draine, B. T., & Anderson, N. E. 1985, ApJ, 292, 494
Draine, B. T., & Lee, H.-M. 1984, ApJ, 285, 89
Dressel, L. L., & Condon, J. J. 1976, ApJS, 31, 187
Faber, S. M., & Gallagher, J. S. 1976, ApJ, 204, 365
Faber, S. M., Wegner, G., Burstein, D., Davies, R. L., Dressler, A., Lynden-Bell, D., & Terlevich, R. J. 1989, ApJS, 69, 763
Frogel, J. A. 1990, paper presented at the ESO/CTIO Workshop, Bulges of Galaxies, unpublished
Frogel, J. A., Persson, S. E., Aaronson, M., Becklin, E. E., Matthews K., & Neugebauer, G. 1975, ApJ, 200, L123
Frogel, J. A., Persson, S. E., Aaronson, M., & Matthews, K. 1978, ApJ, 220, 75
Frogel, J. A., Terndrup, D. M., Blanco, V. M., & Whitford, A. E. 1990, ApJ, 353, 494
Frogel, J. A., & Whitford, A. E. 1987, ApJ, 320, 199
Gezari, D. Y., Schmitz, M., & Mead, J. M. 1987, NASA Ref. Publ. 1196
Gillett, F. C., de Jong, T., Neugebauer, G., Rice, W. L., & Emerson, J. P. 1988, AJ, 96, 116
Glass, I. S. 1976, MNRAS, 175, 191
———. 1984, MNRAS, 211, 461
Glass, I. S., & Moorwood, A. F. M. 1985, MNRAS, 214, 429
Goudfrooij, P., Nørgaard-Nielsen, H. U., Hansen, L., Jørgensen, H. E., & de Jong, T. 1990, A&A, 228, L9
Gordon, M. A. 1990, ApJ, 350, L29
Grasdalen, G. L. 1975, ApJ, 195, 605
Grasdalen, G. L., & Joyce, R. R. 1976, ApJ, 208, 317
Griersmith, D., Hyland, A. R., & Jones, T. J. 1982, AJ, 87, 1106
Gunn, J. E., & Dressler, A. 1989, in Towards Understanding Galaxies at High Redshift, ed. R. Kron & A. Renzini (Dordrecht: Kluwer) 227
Gunn, J. E., Stryker, L. L., & Tinsley, B. M. 1981, ApJ, 249, 48
Helou, G. 1986, ApJ, 311, L33
Helou, G., Khan, I. R., Malek, L., & Boehmer, L. 1988, ApJS, 68, 151
Hill, G. J., Becklin, E. E., & Wynn-Williams, C. G. 1988, ApJ, 330, 737
Huchra, J. P. 1977, ApJS, 35, 171
Impey, C. D. 1983, MNRAS, 202, 397
Impey, C. D., Wynn-Williams, C. G., & Becklin, E. E. 1986, ApJ, 309, 572 (Paper I)
———. 1990, ApJ, 356, 62 (Paper II)
IRAS Catalogs and Atlases: Explanatory Supplement. 1988, ed. C. A. Beichman, G. Neugebauer, H. J. Habing, P. E. Clegg, & T. J. Chester (Washington, DC: GPO)
IRAS Point Source Catalog, Version 2. 1988, Joint *IRAS* Science Working Group (Washington, DC: GPO)
Johnson, H. L. 1966, ARA&A, 4, 193
Jones, T. J., & Hyland, A. R. 1982, MNRAS, 200, 509
Judge, P. G. 1989, in IAU Colloq. 106, Evolution of Peculiar Red Giants, ed. H. R. Johnson & B. Zuckerman (Cambridge: Cambridge Univ. Press), 303
Jura, M. 1986, ApJ, 306, 483
Jura, M., Kim, D.-W., Knapp, G. R., & Guhathakurta, P. 1987, ApJ, 312, L11
Killeen, N. E. B., Bicknell, G. V., & Carter, B. 1986, ApJ, 309, 45
Kim, D.-W. 1989, Ph.D. thesis, U.C.L.A
Knapp, G. R. 1992, in preparation
Knapp, G. R., Bies, W. E., & van Gorkom, J. H. 1990, AJ, 99, 476
Knapp, G. R., Guhathakurta, P., Kim, D.-W., & Jura, M. 1989, ApJS, 70, 329
Knapp, G. R., & Morris M. 1985, ApJ, 292, 640
Knapp, G. R., & Patten, B. M. 1991, AJ, 101, 1609
Knapp, G. R., Rauch, K. P., & Wilcots, E. M. 1990, in ASP Conf. Proc. No. 12, The Evolution of the Interstellar Medium, ed. L. Blitz (San Francisco: ASP), 151
Knapp, G. R., Turner, E. L., & Cunniffe, P. E. 1985, AJ, 90, 454
Lees, J. F., Rupen, M. P., Knapp, G. R., & Phillips, T. G. 1991, ApJ, 379, 177
Lépine, J. R. D., Braz, M. A., & Epchtein, N. 1984, A&A, 131, 72

Longmore, A. J., & Sharples, R. M. 1982, MNRAS, 201, 111
Marston, A. P. 1988, MNRAS, 231, 333
Martinez-Roger, C., Phillips, J. P., & Sanchez-Magro, C. 1986, A&A, 161, 237
McAlary, C. W., McLaren, R. A., & Crabtree, D. R. 1979, ApJ, 234, 471
Mould, J. R. 1981, PASP, 93, 25
Neugebauer, G., et al. 1984, ApJ, 278, L1
O'Connell, R. W. 1986, in Stellar Populations, ed. C. A. Norman, A. Renzini, & M. Tosi, (Cambridge: Cambridge Univ. Press), 167
Penston, M. V. 1973, MNRAS, 162, 359
Persson, S. E., Cohen, J. G., Sellgren, K., Mould, J., & Frogel, J. A. 1980, ApJ, 240, 779
Persson, S. E., Frogel, J. A., & Aaronson, M. 1979, ApJS, 39, 61
Pickles, A. J. 1985, ApJ, 296, 340
Price, J. S. 1985, ApJ, 297, 652
Rice, W., Lonsdale, C. J., Soifer, B. T., Neugebauer, G., Koplan, E. L., Lloyd, L. A., de Jong, T., & Habing, H. J. 1988, ApJS, 68, 91
Rich, R. M. 1988, AJ, 95, 828
Rieke, G. H., Lebofsky, M. J., & Kemp, J. C. 1982, ApJ, 252, L53
Rose, J. A. 1985, AJ, 90, 1927
Rose, W. K., & Tinsley, B. M. 1974, ApJ, 190, 243
Sandage, A. R., Becklin, E. E., & Neugebauer, G. 1969, ApJ, 157, 55
Schweizer, F. 1987, in IAU Symp. 127, Structure and Dynamics of Elliptical Galaxies, ed. T. de Zeeuw (Dordrecht: Reidel), 109
Selby, M. J., Blackwell, D. E., Petford, A. D., & Shallis, M. J. 1980, MNRAS, 193, 111
Sellgren, K. 1984, ApJ, 277, 623
Sharples, R. M., Carter, D., Hawarden, T. G., & Longmore, A. J. 1983, MNRAS, 202, 37
Soifer, B. T., Rice, W. L., Mould, J. R., Gillett, F. C., Rowan-Robinson, M., & Habing, H. J. 1986, ApJ, 304, 651
Sparks, W. B., Hough, J. H., Axon, D. J., & Bailey, J. 1986, MNRAS, 218, 429
Tanaguchi, Y., & Watanabe, M. 1987, ApJ, 313, 89
Terndrup, D. M., Frogel, J. A., & Whitford, A. E. 1990, ApJ, 357, 453
Thuan, T. X., & Martin, G. E. 1981, ApJ, 247, 823
Tinsley, B. M., & Gunn, J. E. 1976, ApJ, 203, 52
van den Bergh, S. 1980, PASP, 92, 409
Walsh, D. E. P. 1990, Ph.D. thesis, Princeton Univ.
Walsh, D. E. P., Knapp, G. R., Wrobel, J. M., & Kim, D.-W. 1989, ApJ, 337, 209
Walsh, J. R., & White, N. J. 1982, Observatory, 102, 78
Wannier, P. G., & Sahai, R. 1986, ApJ, 311, 335
Willner, S. P., Elvis, M., Fabbiano, G., Lawrence, A., & Ward, M. J. 1985, ApJ, 299, 443
Wrobel, J. M., & Heeschen, D. S. 1992, ApJS, submitted
Wynn-Williams, C. G., & Becklin, E. E. 1985, ApJ, 290, 108
Zuckerman, B., & Dyck, H. M. 1986a, ApJ, 304, 394
———. 1986b, ApJ, 311, 345
———. 1989, A&A, 209, 119